THE UNIVERSITY OF MICHIGAN

COLLEGE OF ENGINEERING
Department of Mechanical Engineering
Heat Transfer and Thermodynamics Laboratory

Progress Report No. 5

(For the Period August 1962-November 1962)

PRESSURIZATION OF LIQUID OXYGEN CONTAINERS

J. A. Clark
H. Merte, Jr.
V. S. Arpaci
W. J. Yang
P. S. Larsen
E. Lewis
H. Barakat
B. Bailey
D. Rop
L. Chen

ORA Project 04268

under contract with:

NATIONAL AERONAUTICS AND SPACE ADMINISTRATION
GEORGE C. MARSHALL SPACE FLIGHT CENTER
CONTRACT NO. NAS-8-825
HUNTSVILLE, ALABAMA

administered through:

OFFICE OF RESEARCH ADMINISTRATION ANN ARBOR

February 1963

TABLE OF CONTENTS

TABLE OF CONTENTS (Concluded)

LIST OF ILLUSTRATIONS

NOMENCLATURE

A	Interfacial area
$A'(\lambda)$	def. by Eq. (40)
$A''(\lambda)$	def. by Eq. (41)
$B_i(\lambda)$	def. by Eq. (49), i = 1,2,3,...
b	constant def. by Eq. (6)
C_p	molal specific heat
C_i	concentration of i-th component (on mole basis)
$D_i(\lambda)$	def. by Eq. (50), i = 1,2,3...
$\mathscr{D}$	mass diffusivity
f,F	functions of time
h_{fg}	heat of evaporation (or condensation) per mole
h	coefficient of heat transfer
k	thermal conductivity
K	form factor for rising bubble
M	molecular weight
N	mole flux
N_T	total interfacial mass transfer rate, def. by Eq. (53).
n	parameter, def. by Eq. (4)
P	nondimensional bubble radius R/R_o
q	interfacial heat transfer rate
Q	relative nondimensional bubble size $(P-P_o)/(P_\infty-P_o)$
R	bubble radius

NOMENCLATURE (Continued)

Re	Reynolds number
t	time
$t(x,\Theta)$	wall temperature
T	temperature
u	velocity, terminal bubble velocity
v	velocity of interface during discharge
w	nondimensional bubble radius P/P_∞
X(t)	location of interface at time t
x	distance from initial position of the liquid-vapor interface, positive in the direction of vapor
y	space coordinate along liquid film
z	space coordinate into liquid film
α	thermal diffusivity
γ_t	def. by Eq. (42b)
δ_t	def. by Eq. (42a)
δ	property group $(\rho'' h_{fg})/(\rho' C_p')$
ϵ	b_1/b_2 def. by Eq. (11)
λ	constant characterizing the interfacial movement
λ_o	property group $(T_A-T_B)/\delta$
ν	kinematic viscosity
ρ	density
σ_t	def. by Eq. (42c)
Θ	nondimensional temperature $(T-T_B)/(T_A-T_B)$, time in Eq.'s (1) to (11)
τ	nondimensional time $\alpha t/R_o^2$; $(b_1+b_2)\,\Theta$ def. by Eq. (11)

Subscripts

A	component A
b	bulk liquid
B	component B
e	exposure
g	gas
i	component i, i = 1,2,3,...
p	periferal
s	at the surface
sub	subcooling
w	wall
o	initial
∞	at a distance from the interface; asymptotic value

Superscripts

()'	liquid
()"	vapor, gas
$\overline{()}$	mean value
$\dot{()}$	time derivative

ABSTRACT

Experimental runs have been completed on the determination of condensation of pressurant during pressurized-discharge. The results indicate that from 27% to 35% of the inlet flow of pressurant condenses for small tanks. Inlet pressurant temperatures were 70°F and 35°F and the condensation did not appear to be significantly influenced by this variation.

Preliminary analysis of Saturn test runs 51 and 94 have been completed. Theoretical prediction of mean gas temperature at the end of discharge agreed within 6 to 16% of test data. More test data is expected for further analysis.

The results of measurements with the ball-drop accelerometer are presented under free fall and fractional gravity conditions. Because of the inability of this device to measure acceleration continuously during the test drop, a commercial accelerometer capable of furnishing this continuous data is under procurement.

Data are presented for boiling heat transfer to saturated liquid nitrogen from a sphere in the film, transition, maximum, and nucleate regions at fractional gravities of $a/g = 0.20$ and $a/g = 0.33$.

Results are presented of the effect of acceleration of up to $a/g = 19$ on nucleate boiling heat transfer of liquid nitrogen at heat fluxes of $q/A = 10{,}200$ Btu/hr-ft^2 and $q/A = 5{,}100$ Btu/hr-ft^2. The behavior is similar to that previously observed with water as the test fluid.

The dynamic growth of a single inert gas bubble moving through a volatile liquid with constant velocity is predicted from an approximate analysis. Comparison is made with previous results for a stationary bubble, confirming the significance of the translatory bubble motion for the rapid mass transfer assumed in the lumped analysis. Experimental apparatus is under construction.

The exact solutions for time-dependent temperature and concentration distribution and the interfacial heat and mass transfer rates (condensation or evaporation) are derived for a suddenly pressurized, multi-component liquid-vapor system. It is shown that if the ratio of $\rho C_p k$ of the vapor and the liquid regions is small and the temperature difference between the vapor and the liquid regions is also small, then the interfacial mass transfer rate may be written in a simple linearized form. Expressions for one- and two-component systems are also given as special cases.

I. OPTIMIZATION OF PRESSURIZED DISCHARGE-PROCESSES IN CRYOGENIC CONTAINERS

A. Experimental Program

1. MEASUREMENT OF GAS CONDENSATION DURING PRESSURIZED-DISCHARGE

During the process of pressurized-discharge it is possible that some of the inlet pressurant condenses on the cold internal surfaces of a tank, including the gas-liquid interface. In order to determine whether this is the case and to estimate its magnitude, experimental apparatus was set up to determine the necessary quantities. The apparatus used was the 1-ft-diam, 3-ft-long aluminum container described in Refs. 1 and 2 and altered as indicated in Ref. 3 to include continuous measurement and recording of the flow of pressurant. The measurements were made using a Rockwell Model 800 positive-displacement gas meter installed in the inlet gas line just upstream from the chromalox electrical heaters shown in Fig. 30, Ref. 2. Continuous recording of this measurement was accomplished by a potentiometer mounted to an extension on the rotating portion of the gas meter shaft and fed into the Sanborn recorder.

Liquid levels immediately prior to pressurization and at the end of a run were measured by the liquid thermocouples which indicate a steep rise in temperature as the liquid interface passes. A special thermocouple was placed in the neck of the discharge pipe at the bottom of the container to provide an indication of the liquid level at the end of the run. The ullage mass was determined from the gaseous volume above the initial liquid level and the saturated vapor density at the initial pressure. The residual mass in the container was calculated from the gaseous volume above the final liquid level and the mean gas density was calculated from the gas space temperatures as measured by the fixed thermocouples in the gas space. Corrections for net gas volume were made to account for the presence of support pipes, floats, and other items mounted inside the container. All runs were made using gaseous nitrogen as a pressurant over liquid nitrogen. The initial pressure was approximately 1 atmosphere and discharge was at 50 psia. Heat transfer from the container was with the ambient, the annular guard container being removed for all runs. All gas space temperatures were measured using a model 1012 Minneapolis-Honeywell "Visicorder."

The quantity of gas condensed (or evaporated) during a run was computed from the following equation:

$$\Delta m = m_{\text{pressurant}} + m_{\text{ullage}} - m_{\text{residual}}$$

where

$m_{pressurant}$ is the mass of gaseous pressurant introduced into container

m_{ullage} is the mass of gas initially in ullage volume

$m_{residual}$ is the mass of gas in container at the end of discharge

Hence, a positive value of Δm indicates a net condensation of gas inside the gas space during discharge.

The results of three runs are given in Figs. 1, 2, and 3. These show the quantity Δm as a function of time of discharge for inlet gas temperatures of 70°F, 72°F and 35°F. As may be seen from the curves a net condensation is indicated. No significant influence of inlet gas temperature is observed. It is estimated that the uncertainty in Δm is approximately $\pm$ 0.05 lbm. The ullage mass was 0.040 lbm in each run.

The conclusion from these data is that net condensation does occur in the pressurized-discharge process. For a container of this size the percentage condensed ranged from 27% to 35% of the inlet gas. For larger-sized containers this quantity would be expected to be a smaller percent.

2. ANALYSIS OF SATURN DATA

Preliminary analysis of Saturn test runs 51-44, 51-54, 95-19, 95-20, 95-23, 95-29, 95-30, 95-31, 95-32, 95-33, 95-35, and 95-36 have been completed. Because the data from these runs are being repeated with new instrumentation, detailed results are not available as yet.

The analysis consisted of computing the final gas temperature distribution in the Saturn tank from the theory in Ref. 4 using the test input conditions. The results of this calculation were expressed in terms of a mean gas temperature at the end of discharge, which was compared with the temperature resulting from the theory. Tentative conclusions indicate that the gas temperature distribution in the tank is only approximated by the theory but that the final mean temperature is predicted within 6 to 16% of that measured. The theoretical solution (Ref. 4) requires that the time-dependent inlet gas temperature be known at the level corresponding to the initial liquid level. In this analysis the inlet gas temperature was taken as that corresponding to TA1 for the 51-series runs and the 95-series runs. Such a temperature may be satisfactorily used since the purpose of the comparison is to check the validity of the theory applied to large containers which has been successfully employed on small containers.

A summary of results to date is given in Table I.

TABLE 1

SUMMARY OF PRELIMIMINARY ANALYSIS OF SATURN DATA

Test Number	Pre-Pressurant	Pressurant	T_m Calculated	T_m Measured	Ratio $\frac{T_m \text{ CAL}}{T_m \text{ MEAS}}$
			Centerline		
51-44	N_2	O_2	362R	326R	1.110
			Radial Average		
			365	326	1.120
51-54	N_2	O_2	360	310	1.167
95-19	He	O_2	343	322	1.065
95-20	He	O_2	333	313	1.064
95-23	N_2	O_2	339	319	1.063
95-29	N_2	O_2	344	318	1.082
95-30	He	O_2	338	291	1.162
			322	291	1.107
95-31	-	O_2	180	169	1.065
95-32	He	-			
95-33	He	He			
95-35	He	O_2	307	280	1.096
95-36	He	O_2	270	240	1.125

B. Analytical Program

In the last progress report on integral procedure applicable to complicated problems which cannot be handled by exact analytical methods was developed. The accuracy of the procedure is checked by a problem whose exact solution is already known. The problem is the insulated container subject to sudden temperature change at the inlet temperature of the pressurant fluid.

The integral procedure will now be used for the same problem including the axial conduction into the fluid.

The wall energy equation remains the same:

$$\frac{d}{d\Theta}\int_0^{v\Theta} \rho_w C_w A_w t\,dx = \int_0^{v\Theta} hP\,dx(T - t) \qquad (1)$$

However, the fluid energy equation, including the axial conduction (Fig. 27a), becomes

$$\frac{d}{d\theta}\int_0^{v\theta} \rho A dx C T \;=\; \rho A v C T_g - \int_0^{v\theta} hP dx (T - t) + kA\left(\frac{\partial T}{\partial X}\right)_{x=v\theta} . \qquad (2)$$

Here, assuming the inlet is insulated, the axial conduction at the inlet of the container is neglected.

The selected profile for the wall,

$$t(x,\theta) \;=\; \left[\left(\frac{x}{v\theta}\right) - 1\right]^2 f_2(\theta) \qquad (3)$$

is the same as that for the zero conduction case. But when the axial conduction (Fig. 27b) is included, the fluid profile may be written in the form

$$T(x,\theta) \;=\; T_g + \left(\frac{x}{v\theta}\right)\left[\left(\frac{x}{v\theta}\right) - 2\right]\left[T_g - f_1(\theta)\right] - f_1(\theta)\left(\frac{x}{v\theta}\right)^n \qquad (4)$$

where n is a parameter and is to a large extent arbitrary provided $n \geq 2$. Thus the effect of axial conduction is introduced by two additional terms, one in the energy equation and the other in the assumed profile. Early attempts indicate that the additional term of the energy equation introduces considerable difficulty. As a first approximation to the problem, however, this term may be ignored and is justified for the final portion of the pressurized discharge.

Hence, substituting Eqs. (3) and (4) into Eqs. (1) and (2) and using the definitions

$$F_1 \;=\; \left[(T_g - f_1) + \frac{3f_1}{2(n+1)}\right]\theta \quad , \quad F_2 \;=\; f_2\theta \qquad (5)$$

results in the simulataneous differential equations

$$\begin{aligned} \frac{dF_1}{d\theta} + b_1F_1 - \frac{1}{2}b_1F_2 &= \frac{3}{2}b_1 T_g\theta \quad , \\ \frac{dF_2}{d\theta} + b_2F_2 - 2b_2F_1 &= -3b_2T_g\theta \end{aligned} \qquad (6)$$

together with

$$F_1(0) = 0 \quad , \quad F_2(0) = 0 \tag{7}$$

The solution of Eq. (6), subject to initial conditions given by Eq. (7), is

$$\frac{F_1}{b_1} = \frac{F_2}{b_2} = \frac{3}{2} \frac{T_e}{(b_1 + b_2)^2} \left[e^{-(b_1 + b_2)\theta} + (b_1 + b_2)\theta - 1 \right] \tag{8}$$

If desired, combination of Eqs. (3), (4), (5) and (8) gives the temperature variation of the wall and the fluid. However, only the case where the ratio of the interfacial heat transfer to the peripheral heat transfer is significant will be considered. Noting that the interfacial heat transfer

$$Q_i = - kA \left(\frac{\partial T}{\partial x} \right)_{x = v\theta} \tag{9}$$

and the peripheral heat transfer

$$Q_p = \int_0^{v\theta} hP dx (T - t) \tag{10}$$

The ratio of the interfacial heat transfer to the peripheral heat transfer may be obtained in the form

$$\frac{Q_i}{Q_p} = \left(\frac{n+1}{n-1/2} \right) \left(\frac{\alpha hP}{\rho_w C_w A_w v} \right) \frac{(1+\epsilon)(1 + 1/\epsilon)}{\tau^2} \left[\frac{1 - \frac{3/2}{(1+1/\epsilon)\tau} (e^{-\tau} + \tau - 1)}{1 - 2\left(1 - \frac{3/2}{1+\epsilon}\right)(e^{-\tau} + \tau - 1)} \right] \tag{11}$$

where $\tau = (b_1+b_2)\theta$ and $\epsilon = b_1/b_2$. The result is shown as functions of τ and ϵ in Fig. 28.

The next quarter will be spent on the improvement of the foregoing integral method, and on comparison of the results with those obtained by the analog computer.

II. BOILING OF A CRYOGENIC FLUID UNDER REDUCED GRAVITY

A. Measurement of Acceleration

1. BALL-DROP ACCELEROMETER

In the previous progress report[3] the theory behind the design of a simple ball-drop accelerometer was presented. The electrical and mechanical details of this accelerometer are shown in Fig. 4. The ball is held in contact with the upper plate by means of a 0.002-in.-diam nichrome wire attached to a spring, and is released by discharging a condenser through this wire, melting (or vaporizing) it. When the ball leaves contact with the upper plate it breaks an electrical circuit, which starts an electronic counter. When it makes contact with the lower plate it completes another electrical circuit, which stops the counter. The entire discharge and counting operations are monitored on a dual-beam cathode-ray oscillograph, and the oscillograph record is recorded on film. This check is used to verify that the counter reading is the ball-drop time, and not the consequence of spurious voltage pickups.

The condensers are initially charged to a level of 150 v from an external voltage supply. An interlock system is used to prevent their discharge prior to test package release. Triggering is accomplished by tripping a microswitch at a predetermined distance from the test package release point. This distance can be varied to indicate the variation in package acceleration with distance fallen, which may be caused by variations in air drag and guide wire drag for free fall, and by air drag, guide wire drag, and pulley friction for partial gravity drops. The value of the dimensionless effective force field present on the falling platform, a_{app}/g, as determined from the counter reading is an average value over the ball drop-time, which varies from 0.023 sec for a value of a_{app}/g of 1.0, through 0.228 sec for a_{app}/g of 0.01, to infinity for a_{app}/g of 0. (For the application described here, the effective maximum ball-drop time is 1.4 sec the time during which the package is in free fall.)

2. MEASUREMENTS

A series of five tests was conducted with the ball-drop accelerometer at $a/g = 1$ to provide a comparison between the known and measured acceleration due to gravity. From Eq. 43 of Ref. 3, the measured acceleration is

$$g_m = \frac{2(\Delta y)}{(\Delta t)^2} \quad .$$

In all cases $\Delta y = 0.1035$ in. Table II gives the results of the tests.

TABLE II

RESULTS OF BALL-DROP ACCELEROMETER TESTS AT a/g = 1

Test	t_{ms}	g_m ft/sec^2	% Error
1	22.63	33.19	3.2
2	22.90	32.81	2.0
3	22.33	34.51	7.3
4	22.83	33.02	2.7
5	22.91	32.79	2.0
Average	22.72	33.34	3.7

For all cases, the measured acceleration is greater than the gravitational acceleration. With standard gravity, $\Delta t = 23.13$ msec for $\Delta y = 0.1035$ in., with the measured time intervals always being less than this. The electronic counter has a least count of 10 μsec, so the discrepancy is not due to readability. Instead it is believed that the initiation of the counting interval is delayed slightly due to arcing, as the sphere breaks contact with the upper surface upon release. The persistence of the arc is variable and may account for the scatter in the measurements, which amounts to an uncertainty in the drop distance Δy.

Since the accelerometer was intended for use under free fall and fractional gravity, the same relative errors can be tolerated if they remain consistent under these conditions.

Figure 5 shows the measurements obtained with the accelerometer mounted on the test platform, and the test platform under free fall conditions. The abscissa represents the drop distance of the test platform at which time a microswitch caused the ball in the accelerometer to be released. Also included for reference are the predicted values of local acceleration for the test platform configuration, assuming a drag coefficient $C_D = 1$ and assuming both constant guide wire drag $F_D = 0$ and $F_D = 1$ lbf. It is observed that the majority of data points fall within these lines. The spurious data obtained near the test platform release point are believed to be due to the release of elastic energy under 1g stored in the frame of the test platform. The guide wire drag may reasonably be expected to vary from point to point and run to run; therefore scatter in the measurements is likely.

Figure 6 shows the measurements obtained with the accelerometer and the test

platform subjected to several fractional gravities by means of a counterweight. The scatter of the data under these conditions appears appreciable, particularly at the higher fractional gravities. It is possible that the data represent actual variations in the force field present on the test platform. From the free-fall data, the test platform guide wire and air resistance should contribute drag equivalent to less than $a/g = 0.04$. Some additional drag may be introduced by the counterweight guide wires and pulleys.

Another possible cause of the variations may be oscillations induced upon release by the energy stored in the cable connecting the test platform and counterweight, the system acting as a modified two-mass-spring system. With no damping and assuming that the cable would sustain compressive as well as tensile loading, the acceleration of the test platform would sinusoidally oscillate, giving from zero to twice the nominal steady-state acceleration. In the region of the peak heat flux, where heat flux has exhibited a gravity-sensitive behavior, the time-temperature data have shown this oscillatory nature to some extent (e.g., Fig. 7).

In view of the limitation of the ball-drop accelerometer—that it is able to furnish only an average value over a short distance—an accelerometer having capabilities for continuous measurements during the test package drop period appears to be necessary. Accordingly, a Kistler Model 30351 Servo-Accelerometer is under procurement. This unit will have a range of $\pm$ 1.0 g, is capable of withstanding impacts up to 250 g, has a voltage sensitivity of 5.0 volts/g with a resolution of 0.0001 g, and a natural frequency of 150 cps. It is anticipated that this unit will be mounted on the test platform, and that continuous measurements of acceleration will be recorded simultaneously with temperature.

B. Additional Data

Data have been obtained and are presented below for boiling of saturated liquid nitrogen from the 1-in.diam sphere at nominal fractional gravities of $a/g = 0.2$ and $a/g = 0.33$, from nucleate to film boiling.

Nitrogen with purities better than 99% was used in all cases. The standard curves at $a/g = 1$ and $a/g \approx 0$, based on earlier data, are reproduced for reference. It will be noted that a distinct shift of the data in the transition region has occurred, and is believed due to the current use of pure nitrogen.

Except in the film boiling region, the data were reduced by the digital computer. Experience has shown that it is necessary to use discretion in selecting the time-temperature data which serve as inputs to the computer program. As described in Ref. 3, the program takes 5 data points at a time and fits a 5-constant polynomial through these points for interpolation purposes. If the data points are not smooth, a 5-constant polynomial is inadequate and rather severe fluctuations occur in the computed heat flux. It was therefore found necessary to graphically smooth the input data somewhat. Because of this smoothing, the

most cases the changes in input temperature amounted to less than 0.2°F, close to the readability of the recorded data. The resulting heat flux computed might then be interpreted as representing short time-averaged values.

Figure 7 shows the time-temperature data for a particular test run as taken from the recording, along with a faired curve through the daga. Both the raw and faired data were used as inputs to the digital computer. Comparisons between the results are given in Fig. 9, with severe fluctuations arising from the use of the raw data.

1. $a/g = 0.2$ (Nominal)

With the test platform mass of 121.5 lbm and the empty counterweight cylinder mass of 11.3 lbm, the theoretical fractional gravity on the test platform is $a/g = 0.17$. Based on the results of Fig. 6 the nominal value of $a/g = 0.2$ will be used until continuous measurements of acceleration are available. The time of exposure to the new force field has increased from 1.4 sec for $a/g \approx 0$ to 1.6 sec for $a/g = 0.2$.

(a) Film Boiling.—Figure 9 shows the heat flux—temperature difference data for film boiling obtained with the fractional gravity of $a/g = 0.2$. The points at $a/g = 1$ were evaluated in all cases from data taken immediately prior to release of the test platform, and agree with previous film boiling data.

For reference, the film boiling correlation of Frederking and Clark,[5] given here as Eq. (12) is included.

$$\frac{\bar{h}D_o}{k_f} = 0.15 \left[\frac{D_o^3 \rho_f (\rho_\ell - \rho_f) g}{\mu_f^2} \left(\frac{C_p \mu}{h} \right)_f \frac{h_{fg}}{C_p \Delta t_o} \left(1 + 0.5 \frac{C_p \Delta t_o}{h_{fg}} \right) \right]^{1/3} \qquad (12)$$

From this correlation heat flux is a function of acceleration $q/A \propto (a/g)^{1/3}$, which is in good agreement with the data. The film boiling correlation derived by Bromley[6] gives the relation $q/a \propto (a/g)^{1/4}$, and that derived by Berensen[7] gives $q/A \propto (a/g)^{3/8}$. When data covering a wider range of fractional gravities with film boiling are available, these various correlations will be examined in greater detail to discover which, if any, provide more realistic estimates of heat flux.

(a) Nucleate and Transition Boiling.—Figures 10 and 11 show data obtained when the test platform was released while boiling was in the transition or nucleate regions. In Run 34, Fig. 10, the peak heat flux is considerably lower than that obtained with previous data and in Run 35, Fig. 11. The tests in these two runs were conducted with the same sphere and instrumentation but on different days. Given the consistency of the film boiling data obtained in Run 34, Fig. 9, no

explanation exists for the discrepancy in Fig. 10. However, since the low value of the peak heat flux has not been reproduced, the data of Fig. 10 should be discounted.

In Fig. 11, a distinct shift in the transition and nucleate region data at a/g = 1 is noted. This is attributed to the present use of pure nitrogen, which will be continued.

2. a/g = 0.33 (Nominal)

With the test platform mass of 121.5 lbm and the counterweight mass of 21.3 lbm, the theoretical fractional gravity on the test platform is a/g = 0.30. Again, based on the results of Fig. 6, the nominal value of a/g = 0.33 will be used. The time of fall is now 1.75 seconds.

(a) Film Boiling.—In Fig. 12 the data are plotted for film boiling at a/g = 1.0 and a/g = 0.33 along with the correlation of Frederking and Clark.[5]

(b) Nucleate and Transition Boiling.—Heat flux versus temperature difference is plotted in Fig. 13 for a/g = 1 and a/g = 0.33. The shift in the transition region at a/g = 1 is quite pronounced. Insufficient data were obtained in this case to show the peak heat flux at a/g = 1.

The nucleate boiling characteristics at a/g = 1 and a/g = 0.33 are the same, indicating the insensitivity of nucleate boiling to gravity. The slope in the nucleate boiling region is greater than that obtained with impure nitrogen.

3. MAXIMUM HEAT FLUX DATA

In order to show more clearly the influence of fractional gravities on the peak heat flux, the maximum values of heat flux and the corresponding values of temperature difference are plotted in Fig. 14. Also included are the values of peak heat flux and critical temperature difference predicted from the correlations by Chang and Snyder.[8] Since the predicted value of heat flux at a/g = 1 is high, being perhaps an indication that the empirical constant may be too large, a more graphical representation of the influence of fractional gravity is obtained by normalizing the correlation to agree with the experimental values at a/g = 1. The corresponding values of the normalized maximum heat flux at fractional gravities are also plotted on Fig. 14, and reasonable agreement with experimental values is noted at a/g = 0.33 and a/g = 0.2. The experimental value of peak heat flux coincides with the normalized correlation for a/g = 0.03, which is in the range of the measured accelerations shown in Fig. 5.

C. Future Work

When the accelerometer is received it will be installed on the test platform and all tests will be monitored continuously. Some of the previous tests may be rerun with the accelerometer.

Tests at the fractional gravity of $a/g = 0.6$ have been conducted but the data are not yet reduced. These tests will be reported during the next reporting period.

Planning is underway for obtaining data with subcooled liquid nitrogen.

III. HEAT TRANSFER TO A CRYOGENIC FLUID IN AN ACCELERATING SYSTEM

A. General

The main heater in the test vessel has been repaired. A short circuit occurred when the mica insulating the heater ribbon from the copper heater disc failed at a corner where the ribbon emerged from the slot. To repair the heater without a major disassembly it was necessary to bypass the ribbon in one of the slots near the terminal connection. This amounts to less than 3% of the total heater length, and the copper is sufficiently thick so that any non-uniformity in heat flux is essentially smoothed out at the boiling surface.

At the time of disassembly it was noted that the screws attaching the heater assembly to the cylindrical side walls of the inner test vessel were loose, indicating a possible leak of liquid nitrogen. Such a leak would account for the low temperature difference (approximately 2°F) observed between the underside of the main heater and the lower guard heater (see Fig. 76 of Ref. 2).

The gasket between the skirt and the lower side wall flange was replaced and the screws tightened after cooling to liquid nitrogen temperatures. Subsequent observations under test conditions, described below, tend to verify that leaks had been present. However, it is not felt that data taken with the leaks present should be discarded on this account, since the temperature difference across the underside of the main heater had been small and this is a necessary condition for accurate measurement of heat flux. A number of changes, also described below, were necessary before the small temperature difference could be achieved again.

Provision was made so that the main heater and both the skirt guard heater and the underside guard heater would all be active. The wiring diagram is shown in Fig. 15. Also, the styrofoam insulation lining the outer test vessel was cemented into a continuous piece for better isolation of the inner test vessel from the ambient.

Several preliminary tests were conducted with the inner test vessel removed from the outer vessel in order to check for satisfactory operation of the heaters. The test vessel was then reinstalled in the outer vessel.

B. Test Results

The liquid nitrogen used in all subsequent tests was of commercial high purity and was obtained from the Linde Company. Due to a temporarily defective analyzer it was not possible to measure the purity for the tests reported below, but previous measurements indicate that the purity should be better than 98%.

1. RUN 26. a/g = 1, VARIABLE HEAT FLUX

In order to compare on a common basis the effect of acceleration at various levels of heat flux, the behavior of heater surface superheat must be determined as a function of heat flux at a/g = 1. Fig. 16 is a plot of the time-temperature data for Run 26. The temperature difference between the heater surface and the skirt guard heater, was maintained at 0.

It is noted that as heat flux increased the temperature difference across the heater bottom, ΔT_B, decreased from $\Delta T_B = -17°F$ at q/A = 0 to $\Delta T_B = 0$ at q/A = 30,000 Btu/hr-ft^2. Referring to the sketch in Fig. 21, ΔT_B is defined by

$$\Delta T_B = T_{HB} - T_B$$

A minus value of ΔT_B means that the lower guard heater is higher in temperature than the main heater, indicating that heat transfer is possible from the ambient to the heater underside. The presence in Run 26 of a ΔT_B higher than that in previous data tends to verify the existence of a liquid nitrogen leak which had served to cool the guard heater. Because it was uncertain whether a large value of ΔT_B would have a detrimental effect on the data, several tests were conducted with the system under rotation.

Figure 17 is a plot of q/A versus $T_H - T_{sat}$ for Run 26 along with data previously presented at a/g = 1. The presence of some scatter of the data obtained with high purity liquid nitrogen is representative of the non-reproducible nature of the boiling process. A consistent trend is present, however, in that the slope is more steep than that of previous data obtained with impure liquid nitrogen.

2. RUN 27. q/A = 10,200 Btu/hr-ft^2

Figure 18 shows the time-temperature data for the various accelerations. It is noted that the heater surface temperature is parallel to the fluid saturation temperature as liquid level changes during acceleration, indicating that $T_H - T_{sat}$ is independent of small changes in hydrostatic pressure at the heater surface. Also, the measured liquid temperatures decrease with decrease in the hydrostatic pressure.

At a/g = 1, the temperature difference across the heater underside, ΔT_B, has an asymptotic value of -13°F. This decreases with increases in acceleration to ΔT_B = -8°F at a/g = 18.3. The decrease is believed to be due to the large buoyant forces present on the vapor, which force the colder, more dense vapor to the bottom of the outer vessel, thus helping to cool the underside guard heater more effectively.

Figure 19 shows the heater surface and liquid nitrogen superheats for the various accelerations. The heater surface superheat increases with increasing acceleration, a phenomenon similar to that found with water.[9] Similar results were obtained in a previous test (Fig. 33 of Ref. 3), except that in the present case the increase is larger and linear. The limited rise in Fig. 33 of Ref. 3, which may be a consequence of the liquid nitrogen leak mentioned earlier, will be checked by additional tests. It is also noted that the liquid superheat decreases with acceleration as a consequence of the mixing induced by large buoyant forces.

3. Run 29. q/A = 5,000 Btu/hr-ft^2

Figure 20 shows the results of a test run similar to Run 27 except that it was made at a lower value of heat flux. As acceleration increases, the heater surface superheat (T_H-T_{sat}) first increases and then decreases, due to the increasing contribution of natural convection. The behavior is similar to that observed on a previous test, shown in Fig. 42 of Ref. 3. Throughout the entire test the values of T_H-T_{sat} were highly stable at a/g = 1 and it was not necessary to normalize the data.

With the liquid nitrogen leak not present, the temperature difference across the heater underside, ΔT_B, increased to ΔT_B = -16°F at a/g = 1. Under acceleration this decreased to ΔT_B = -10°F at a/g = 18.3; it is plotted in the upper portion of Fig. 20.

In this particular test it was also observed that a transient in (T_H - T_{sat}) and ΔT_B occurred at a/g = 1 immediately following operation at each higher acceleration. It is thus possible to show a relationship between T_H-T_{sat} and ΔT_B, as is done in the lower curve of Fig. 20. The change in T_H - T_{sat} should not be interpreted as resulting from the sole influence of ΔT_B, since a change in hydrostatic pressure under acceleration causes a change in temperature level of T_H. The favorable comparison between these data and those of Fig. 42 of Ref. 3, where ΔT_B was less than 2°F, would tend to minimize the effect of ΔT_B on T_H - T_{sat}.

C. Modification of Test Vessel

To minimize the uncertainty of the above-noted effect a concerted effort was made to reduce the value of ΔT_B to a point where it could be maintained

constant at all values of heat flux and accelerations. This was accomplished by forcing the cold boil-off vapor to flow in the vicinity of the underside guard heater before venting to the atmosphere, thus better isolating the guard heater from effects of the ambient.

Figure 21 is a sketch of the modified outer vessel. The major changes consist of the following:

(1) The filling vent is now closed during operation and the boil-off vapor flows down the annulus between the inner test vessel and the sealed styrofoam lining the outer vessel, and out the vent hoses inserted in the lower portion.

(2) The cover of the inner test vessel was removed and the liquid thermocouples and low-level detector suspended within the test vessel so that an integral piece of styrofoam could be cemented to the outer vessel cover to reduce heating of the boil-off vapor by the ambient.

(3) Slots were cut in the styrofoam on which the inner test vessel rested in order to permit more free flow of the boil-off vapors around the under guard heater.

(4) The lower portion of the outer vessel was insulated externally with styrofoam and fiberglas to further reduce heat transfer from the ambient.

D. Future Work

Tests have been conducted at $q/A \approx 10{,}000$ Btu/hr-ft^2 and $q/A \approx 20{,}000$ Btu/hr-ft^2 since the above modifications were made and the data will be reduced and reported during the next period. Test runs will be conducted at $q/A \approx 30{,}000$ Btu/hr-ft^2 and possibly up to $q/A = 40{,}000$ Btu/hr-ft^2.

IV. INJECTION COOLING

A. Bubble Dynamics

1. INTRODUCTION

An outline of the anticipated bubble dynamic studies in connection with the gas injection cooling process was given in Ref. 2, p. 40. The dynamics of the single bubble having no translatory motion was analyzed approximately by means of source theory in Ref. 3, p. 30, under the simplifying assumption of uniform composition in the gas phase at all times. The conclusion of this analysis was that the predicted growth rates were not sufficiently large to justify ignoring the translatory bubble motion. Within the range of subcooling experienced in the injection cooling process, $\Delta\Theta_{sub} = 1 - (T_b-T_B)/(T_A-T_B) = 0...0.5$, a bubble will move several diameters owing to buoyancy forces in the time predicted for only 50% relative bubble growth. Thus, for example, an insoluble gas bubble of initial size R_o = 1/8-in. introduced into liquid oxygen at 3.1 atm, T_b = 178.1°R ($\Delta\Theta_{sub}$ = 0.2), will have reached only 52% of its final equilibrium size after 1-sec exposure ($\tau = 7.3 \times 10^{-3}$ in Fig. 47, Ref. 3). The terminal velocity of a 1/4-in.-diam bubble in liquid oxygen is in the order of u = 0.6 ft/s.[10] The assumption of uniform composition in the gas phase at all times, equal to the average value corresponding to the bubble size, furthermore implies that the above estimate is conservative. The transport by mass diffusion of the evaporing liquid component A from the bubble interface through the gas mixture towards the bubble center indicates that the composition of the gas at the interface is at all times richer in component A than is given by the average value of composition used in the analysis. Hence, the corresponding equilibrium temperature of the bubble interface will be greater, the potential for bubble growth smaller, and the growth rate consequently smaller. This substantiates the need for incorporating the translatory motion of the bubble.

A simplified analysis based on the "falling film" theory has been employed in predicting the dynamics of a single spherical bubble, initially containing a nonsoluble gas and having a constant translatory motion through a volatile quiescent liquid extending to infinity, initially at uniform pressure and temperature.

2. ANALYSIS FOR SINGLE MOVING BUBBLE

When a gas bubble is injected into a liquid column subjected to a gravitational force field it is accelerated by the excess of buoyant force over the drag force, until this excess becomes zero and the terminal velocity, u, is

reached. The shape of the rising bubble and the path followed depend on bubble size and fluid properties and may be classified relative to a bubble Reynolds' Number $Re_D = 2Ru/\nu'$ (Ref. 10, p. 10). Above Re = 2, corresponding to R = 0.002-in. for liquid oxygen, bubbles deviate from the idealized Stokean model of a moving rigid sphere owing to:

Vibration
Non-sphericity
Wake and vortex shedding
Fragmentation
Slip flow at the gas-liquid interface

The range of bubble size of interest ($R \sim 1/8.....1/4$-in.) corresponds to $Re_D >$ 7000 for liquid oxygen.

Two schools of thought have been dominant in the attempts to describe satisfactorily the mass transfer to moving drops or bubbles without accounting for the exact velocity profile next to the interface. The "stagnant film" theory assumes that the bubble is surrounded by a stagnant liquid film of a thickness which is small compared with the bubble size. Outside this film the potential for the transfer process remains constant at the bulk liquid value. The weakness in this theory lies in the difficulty of determining the effective film thickness in question and in the fact that motion of the gas inside the bubble has been observed, indicating that the liquid film probably does not retain its identity.

As a gas bubble rises through a liquid, the gas phase in the bubble is believed to undergo a toroidal motion such that there is essentially no slip between liquid and gas at the interface near which the liquid can be considered in laminar flow. This is equivalent to stating that there is essentially full slip between the liquid and the bubble. As the bubble rises through the liquid, the gas phase at the top of it steadily encounters fresh liquid which moves down over the bubble exposed to the gas until it leaves at the bottom of the bubble. Under the name "penetration" theory, this concept has successfully been employed in the prediction of gas absorption from bubbles rising through a non-volatile liquid. When the exposure time is short the "penetration depth" of the potential distribution for the transfer process into the liquid is so small that the transfer may be treated as a transient diffusion process into a falling liquid film of uniform velocity exposed to a well mixed gas phase. The weakness of this theory lies in the difficulty of ascertaining the actual average exposure time, the velocity distribution in the liquid film, and the mixing in the gas phase. The concept of some surface renewal, however, seems physically meaningful and has been introduced in a more generalized form by Danckwerts[11] for analyzing gas absorption from bubbles in an agitated tank. An average exposure time is arrived at here by considering the frequency function for the fractional rate of surface area renewal to be exponential.

The following model is adopted for predicting the transient growth of a single bubble containing initially a nonsoluble, noncondensing, and chemically nonreactant gas (component B), rising with constant translatory velocity u

through a volatile quiescent liquid (component A) of uniform temperature T_b:

(a) The rate of mass transfer by evaporation of the liquid component A into the gas phase is governed by the rate of heat diffusion through a liquid film falling with uniform velocity u and having an average exposure time $\overline{t}_e$ to the gas phase.

(b) Convective flow perpendicular to the gas-liquid interface resulting from bubble growth is ignored.

(c) The gas-liquid interfacial temperature, T_s, corresponds at all times to that of thermodynamic phase-equilibrium at the liquid pressure and the average gas composition in the bubble.

(d) Heat capacity and compressibility of the gas phase is ignored, and the gas is assumed to be well mixed at all times.

(e) The change in bubble size is assumed not to effect the rise velocity u, which is taken constant to its terminal value corresponding to the initial bubble size.

On the basis of assumptions (c) and (d), bubble size and interfacial liquid temperature are uniquely related. The process is considered quasi-steady by assuming that the interfacial temperature, T_s, remains essentially constant throughout the surface for the average exposure time, $\overline{t}_e$. This is a reasonable assumption since the exposure time is short compared with the time for a significant change of the interface temperature, that is, in the asymptotic stage of growth. This quasi-steady approach also circumvents the inconsistency of assuming uniform interfacial temperature when in fact the surface age varies over the bubble interface.

The analytical model is shown in Fig. 22. The mathematical formulation of heat diffusion from a falling liquid film of velocity u and the initial uniform temperature, T_b, exposed over a distance $y_e = u \cdot t_e$ to a gas such that the interface temperature, T_s, remains constant, is given by

$$u \frac{\partial T}{\partial y} = \alpha \frac{\partial^2 T}{\partial z^2}$$

$$T(0,z) = T_b \qquad (13)$$

$$T(y,\infty) = T_b$$

$$T(y,0) = T_s$$

when the heat diffusion in the y-direction can be neglected compared with the enthalpy flux owing to convection.

The solution being

$$\frac{T_b - T}{T_b - T_s} = \operatorname{erfc} \frac{z}{\sqrt{4\,\alpha\, y/u}} \tag{14}$$

the average heat flux leaving the liquid over the exposure length, y_e, becomes

$$q = \frac{1}{y_e} \int_o^{y_e} k \frac{\partial T(y,o)}{\partial z}\, dy = (T_b - T_s)k \sqrt{\frac{4u}{\pi \alpha y_e}} \tag{15}$$

Ignoring the heat capacity of the gaseous phase, this heat flux facilitates an average molar flux of component A evaporating into the bubble of

$$\overline{N_A''} = \rho'' \frac{T_b - T_s}{\delta} \sqrt{\frac{4\alpha u}{\pi y_e}} \tag{16}$$

where $\delta = (\rho'' h_{fg})/(\rho' C_p')$. By continuity consideration the average molar flux is related to the spherical bubble size, R, as

$$\overline{N_A''} = \rho'' \frac{1}{4\pi R^2} \frac{d}{dt} \left(\frac{4}{3} \pi R^3\right) = \rho'' \dot{R} \tag{17}$$

Introducing next the nondimensional quantities

$$\tau = \alpha t / R_o^2$$

$$P = R/R_o$$

$$\theta = (T - T_B)/T_A - T_B)$$

$$\lambda_o = (T_A - T_B)/\delta$$

and assuming that the exposure time $\bar{t}_e$ is proportional to the bubble size $\bar{t}_e = y_e/u = KR/u$, Eqs. 16 and 17 combine to

$$\frac{\sqrt{P}\, \dot{P}}{(\theta_b - \theta_s)} = 2\lambda_o \sqrt{\frac{uR_o}{\pi \alpha K}} \tag{18}$$

The form factor K relating the average exposure length y_e for flow over a bubble to its radius was taken to K = 2 by Higbie.[12] For constant velocity over the surface of a sphere, however, the analytic value becomes $K = 2(\pi - 2)$. A rigorous evaluation including a given velocity distribution over the surface, e.g., that

resulting from potential flow, is not possible if stagnation points exist.

Equation (15) may be integrated when the temperature variation is specified, giving the bubble growth either as function of time $P = P(\tau)$ or, by assumption (e) above, as function of position $Y = u \cdot t$ above point of injection into the liquid.

For constant interface and liquid bulk temperature, Eq. 18 describes the approximate asymptotic growth of a vapor bubble moving at constant velocity in a boiling, one-component liquid. The result

$$P(\tau) = [1 + 3\lambda_o (\theta_b - \theta_s) \sqrt{(uR_o)/(\pi\alpha K)}\tau]^{2/3} \qquad (19)$$

which for vanishing initial size becomes

$$P(\tau) = [3\lambda_o(\theta_b - \theta_s)]^{2/3}[(uR_o)/(\pi\alpha K)]^{1/3} \tau^{2/3} , \qquad (20)$$

where R_o can be considered an arbitrary normalizing factor, indicates that a moving bubble grows with $\tau^{2/3}$ compared with $\tau^{1/2}$ for the stationary bubble (p. 31 of Ref. 3).

For the case of gas injection, assuming a linear phase-equilibrium approximation $x = \theta$ for the dew curve of the ideal binary mixture of components A and B assumptions (c) and (d) lead to the relationship

$$P^3 = 1/(1 - x_s) = 1/(1 - \theta_s) \qquad (21)$$

Substituting Eq. 21 into Eq. 18 gives

$$\frac{P^{7/2}\,\dot{P}}{1/(1 - \theta_b) - P^3} = 2\lambda_o(1 - \theta_b)\sqrt{(uR_o)/(\pi\alpha K)} \qquad (22)$$

which for non-zero bulk subcooling, $\theta_b < 1$, integrates to

$$\ell n \frac{(1 + w^{3/2})(1 - w_o^{3/2})}{(1 - w^{3/2})(1 + w_o^{3/2})} - 2(w^{3/2} - w_o^{3/2}) = 6\lambda_o w_o^{9/2} \sqrt{\frac{uR_o}{\pi\alpha K}}\,\tau \qquad (23)$$

where $w = P/P_\infty$ is the bubble size normalized with respect to its asymptotic value, $P_\infty = (1 - \theta_b)^{-1/3}$, such that $w_o = P_o/P_\infty = 1/P_\infty$.

For the particular case of a non-soluble gas bubble rising through a saturated liquid ($\Theta_b = 1$), Eq. (22) integrates to

$$P(\tau) = [1 + 9\lambda_o \sqrt{(uR_o)/(\pi\alpha K)}\ \tau]^{2/9} \qquad (24)$$

indicating continued growth ad infinitum. Equation (24) can be considered valid only as long as the change of bubble size does not cause significant changes in the rise velocity u.

In Fig. 23, $Q = (P - P_o)/(P_\infty - P_o)$, which according to Eq. (23) is relative nondimensional bubble growth for a 1/8-in. initial-sized, non-soluble gas bubble moving through liquid oxygen at 3.1 atm with a constant velocity, u = 0.6 ft/s, is compared with the previously obtained approximate results (Fig. 47 of Ref. 3) for a stationary bubble, for a relative subcooling, $\Delta\Theta_{sub} = 1 - \Theta_b$, of 0.2 and 0.4 respectively. The significance of the translatory motion on the bubble growth-rate appears clearly from Fig. 23. This indicates that after 1-sec residence time in liquid oxygen at 3.1 atm at 178.1°R ($\Delta\Theta_{sub} = 0.2$), a 1/4-in.-diam moving bubble will have reached 91% of its final equilibrium size compared with 52% for a stationary bubble.

Thus, accounting for the nonradial liquid flow around the expanding bubbles, the assumption of an equilibrium process utilized in the lumped analysis for the injection cooling process seems justified. That is, for moderate bubble sizes, absence of bubble interferences and coalescence, and gas holdup times in the order of seconds, as normally experienced.

If interference between bubbles is absent an efficiency for the injection process may be defined in terms of column high or exposure time. However, for a more general treatment, bubble interference (laterally and axially) and wall effect must be taken into account. During the next period the axial transient temperature profiles will be examined in liquid columns resulting from the injection of a non-soluble gas with given initial bubble size.

3. EXPERIMENTAL PROGRAM

Construction of apparatus for the experimental study of the dynamics of the single stationary bubble is nearly completed. The view tank has been leak tested and the bubble injector has proved to operate properly. Preliminary measurements on the injector solenoid indicate that bubble formation times of 5-10 ms are likely to be achieved by a Visicorder connected to the electronic switching circuit as shown in Fig. 24. The formation time is adjustable through (a) change of the time constant for the break-relays circuit (resistor R_1), (b) change of injector valve stroke and spring tension, and (c) change of gas pressure in excess of the surrounding liquid. The instrumentation will permit recording of gas temperature and pressure prior to bubble injection, liquid bulk tempera-

ture, liquid pressure at bubble location, and photographic recording of bubble size vs. time.

Construction of apparatus is in progress for the experimental study of the dynamics of a single bubble moving through a volatile liquid owing to buoyancy effects, the liquid having constant temperature and pressure. The constant temperature and pressure condition is conveniently simulated by suspending the bubble in a stream of the liquid flowing vertically downwards through a diffuser at approximately the terminal rise velocity of the bubble. This experimental model permits visual observation of the bubble from a fixed position in space, and simulates fairly well the flow field in the liquid relative to a rising bubble. Figure 25 shows schematically the flow diagram for the recirculation loop, which has a 34-mm ID glass test section for downflow, terminating in the view tank with a divergent conduit (61-mm max. ID) above the bubble injector, from which the bubble to be studied will be injected. A 15-gpm, 80-ft head centrifugal pump, fed from the lower reservoir, discharges into the constant head upper reservoir, which has an overflow to the lower reservoir and is equipped with a 2.5-kw electrical immersion heater. The desired downflow velocity in the test section is attained by discharging the liquid from the constant head upper reservoir through a rotary flowmeter and the main control valve to the lower reservoir. A purification bypass from the pump discharge line to the lower reservoir contains an ion exchanger equipped with a No. 5 Poro-Klean filter. For degassing purposes the upper reservoir is equipped with a water cooled condenser coil, and the pressure in the vapor space of the two reservoirs is equalized through an interconnection line. The system can be maintained at or slightly below atmospheric pressure by means of an ejector-type vacuum pump connected to the vapor space of the upper reservoir. All components in contact with the liquid and its vapor are of stainless steel or Pyrex glass and are equipped with seals and gaskets of Teflon or Neoprene.

The instrumentation will permit the recording of liquid pressure, temperature, and velocity at the test section, as well as the recording of gas pressure and temperature prior to injection of the bubble. The transient bubble size will be photographically recorded. A mirror system used also for the study of the stationary bubble will provide a picture containing two views, 90° apart, of the bubble in addition to the direct view.

Materials are arriving for the recirculation loop, and the structure for its support has been erected.

V. INTERFACE HEAT AND MASS TRANSFER IN A SUDDENLY PRESSURIZED LIQUID-VAPOR SYSTEM

A. Literature Survey

The dynamics of phase growth has attracted considerable attention in boiling, condensation, melting, and solidification in which a substance has a transformation point at which it changes from one phase to another with emission or absorption of heat. The essential feature of such problems is the existence of a moving surface of separation between two phases, with the liberation or absorption of heat on it. Since the thermal properties of the two phases on different sides may be different, the problem is non-linear and the special solutions must be determined.

In the case of melting and solidification, the problem of phase growth is frequently referred to as the problem of Stefan. The movement of the interface is characterized by the well known $x(t) = 2\lambda\sqrt{\alpha t}$ law (radius grows as square root of time), which also represents the growth rate of phase in boiling and condensation.

In boiling heat transfer, the transfer of latent heat from the boiling surface to the liquid is related to the formation and growth of vapor bubbles. In addition, heat may be transferred through the vapor bubble by mass transfer, i.e., some of the heat used to vaporize the liquid near the base of the vapor bubble is carried as vapor to the bubble cup, where it is transferred to the liquid bulk by condensation of the vapor. Thus both heat and mass transfer occur at the bubble surface. This indicates the similarity in mechanism between the bubble growth and the interface heat and mass transfer in the pressurization of the cryogenic fluids.

Lord Rayleigh[13] was the first to formulate the process of bubble growth or collapse as a problem in the hydrodynamics of an incompressible increased fluid. Plesset[14] modified the Rayleigh equation by adding a surface tension term. The approximate solutions for the bubble growth in the asymptotic stage in pure liquids were obtained by Plesset and Zwick[15] by the "thin thermal boundary layer," and by Forster and Zuber[16] by "the point source theory."

For the dynamics of phase growth in a two-phase system of unequal densities, Chambre[17] studied the influence of radial convection on spherically symmetric phase growth controlled by diffusion. Scriven[18] formulated the equations governing spherically symmetric phase growth in an infinite medium for the general case and then simplified them to describe growth controlled by the transport of heat and matter. Exact solutions of the equations are obtained for conditions typical

of bubble growth in the nucleate boiling of pure materials and binary mixtures. The effect of radial convection resulting from unequal phase densities is established. Yang and Clark[19] modified and extended the source theory first proposed by Forster and Zuber by regarding the bubble growth in a binary solution as a simultaneous operation of heat and mass sinks on the bubble surface. The results agree very well with those obtained by Scriven. The idea was also applied to the bubble growth of the presenting gas in the cryogenic fluids.

For the phase change in a suddenly pressurized one-component liquid-vapor system, Thomas and Morse[20] obtained an exact solution for the mass flux of condensate or evaporate across the interface. The interface is assumed to be at the saturation temperature corresponding to the pressure of the pressurant. A similar study was conducted by Knuth,[21] where it was shown that: (1) If for each phase the specific enthalpy of the initial state and that of the saturated state corresponding to the system pressure is small in comparison with the latent heat, then the expression for the evaporation or condensation rate may be written in a simple linearized form; and (2) If the system pressure is not close to the initial pressure of the fluid, then the heat flux in the liquid phase dominates the heat flux in the vapor phase.

B. Formulation of Problem

An insulated container is partially filled with multi-component liquids at T'_∞, the saturation temperature corresponding to the gas pressure P_o. Then suddenly a pressurant consisting of the same components as the liquids is introduced into the container, instantaneously changing the gas pressure to P''_∞ and its temperature to T''_∞. This change in the pressure level is accompanied by condensation or evaporation in which the latent heat is absorbed or supplied. Assuming both the liquid and vapor regions to be semi-infinite in extent, the study is aimed at the solution for the heat flux and the mass flux of condensate or evaporate across the interface and the temperature-time history of the vapor and liquid regions.

According to the characteristics of the system considered, the classification of phase dynamics shown in Table III may be made. The following assumptions are imposed on the solutions:

1. The density ρ, specific heat C_p, and thermal conductivity k are constant for each phase and each component. This is a reasonable assumption if temperature variations within each phase are small.

2. Effects of natural convection do not exist.

3. At the moment of pressurization, the interface temperature immediately adjusts to the saturation temperature T_{sat} corresponding to the system pressure

TABLE III

MODELS FOR INTERFACE HEAT AND MASS TRANSFER IN A MULTI-COMPONENT SYSTEM

Model	Liquid		Gas	
	Heat Transfer	Mass Transfer	Heat Transfer	Mass Transfer
1	No	No	Yes	Yes
2	No	No	Yes	No
3	No	No	No	Yes
4	Yes	No	Yes	Yes
5	Yes	No	Yes	No
6	Yes	No	No	Yes
7	Yes	No	No	No
8	No	Yes	Yes	Yes
9	No	Yes	Yes	No
10	No	Yes	No	Yes
11	No	Yes	No	No
12	Yes	Yes	Yes	Yes
13	Yes	Yes	Yes	No
14	Yes	Yes	No	Yes
15	Yes	Yes	No	No

P''_∞. This contradicts the kinetic theory of gases in that a net mass flux is realized only if there exists a difference between the interface temperature and the saturation temperature corresponding to the vapor pressure at the interface, or if there exists a difference between the vapor pressure at the interface and the saturation pressure corresponding to the interface temperature. However, these differences are believed to be small and may be neglected in the analysis.

4. The mass diffusivity $\mathcal{D}$ for each phase remains unchanged.

5. Ideal vapor and liquid phases are assumed.

With these assumptions, conservation of energy and mass on each phase give the following differential equations for general case, model no. 12 of n-component system.

(a) Temperature distribution

In vapor region:

$$\frac{\partial T''}{\partial t} + u'' \frac{\partial T''}{\partial x} = \alpha'' \frac{\partial^2 T''}{\partial x^2} \tag{25}$$

In liquid region:

$$\frac{\partial T'}{\partial t} = \alpha' \frac{\partial^2 T'}{\partial x^2} \tag{26}$$

(b) Concentration distribution

In vapor region:

$$\frac{\partial C_i''}{\partial t} + u'' \frac{\partial C_i''}{\partial x} = \mathcal{D}_i'' \frac{\partial^2 C_i''}{\partial x^2} \qquad \text{for } i = 1,2,\ldots,n-1 \tag{27}$$

In liquid region:

$$\frac{\partial C_i'}{\partial t} = \mathcal{D}_i' \frac{\partial^2 C_i'}{\partial x^2} \qquad \text{for } i = 1,2,\ldots,n-1 \tag{28}$$

It must be noted that T'', T' and C_i'', C_i' represent the transient components of temperature and concentration respectively. Since the governing differential equations expressed by Eqs. (25) through (28) and the boundary conditions expressed by Eq. (30) are all linear in nature, the dynamic characteristics of the system will not be affected by the initial distribution of temperature and concentration in the system. This statement would not be true if the absolute velocity of the vapor as expressed by Eq. (32) were a function of temperature or concentration.

The origin of the axis is fixed at the initial position of the liquid-vapor interface. x is positive in the direction of the vapor. The absolute velocity of the liquid is 0. The velocity of the vapor is obtained from the equation of continuity and the conservation of mass across the interface as follows:

$$u'' = -\frac{\rho' - \rho''}{\rho''} \frac{dX}{dt} \tag{29}$$

where X(t) is the location of the interface at any instant t. As in cases of melting, solidification, and bubble growth and collapse, it is considered that for the present problem the movement of the interface is also characterized by the square-root-of-time law, that is

$$X(t) = 2\lambda\sqrt{\alpha' t} \tag{30}$$

where λ is a constant characterizing the interfacial movement and is positive for condensation, negative for evaporation. Then the velocities of the interface and the vapor may be expressed respectively as

$$\frac{dX}{dt} = \lambda \sqrt{\frac{\alpha'}{t}} \tag{31}$$

and

$$u'' = - \frac{\rho' - \rho''}{\rho''} \lambda \sqrt{\frac{\alpha'}{t}} \tag{32}$$

The initial and boundary conditions are given by

$$T''(x,o) = T'(x,o) = T'_\infty \tag{33a}$$

$$T''(\infty,t) = T''_\infty \tag{33b}$$

$$T'(-\infty,t) = T'_\infty \tag{33c}$$

$$T''(X,t) = T'(X,t) = T_s \tag{33d}$$

$$k' \frac{\partial T'(X,t)}{\partial x} - k'' \frac{\partial T''(X,t)}{\partial x} = h_{fg} \rho' \frac{dX}{dt} \tag{33e}$$

$$C''_i(x,o) = C''_{i\infty} \tag{33f}$$

$$C''(\infty,t) = C_i''_\infty \tag{33g}$$

$$C'(-2,t) = C''_{i\infty} \tag{33h}$$

$$C''_i(X,t) = C''_{is} \quad , \quad C'_i(X,t) = C'_{is} \tag{33i}$$

$$\mathcal{D}'_i \frac{\partial C'_i(X,t)}{\partial x} - \mathcal{D}''_i \frac{\partial C''_i(X,t)}{\partial x} = \rho' \frac{dx}{dt} \left[\frac{C''_i(X,t)}{\rho''} - \frac{C'_i(X,t)}{\rho'} \right] \tag{33j}$$

Equation (33e) represents the condition for the conservation of energy across the interface under the assumption that the heat of mixing, kinetic energy terms, etc., are negligible. Therefore this equation signifies that the net heat flow

across the interface corresponds to energy evolved or required for the phase change, $h_{fg}\rho'$ (dX/dt). dX/dt is the absolute velocity of the interface, positive for condensation and negative for evaporation. $\rho'(dX/dt)$ is the mass flux of condensate (for positive value), or of evaporate (for negative value). Similarly Eq. (33j) represents the condition for the conservation of mass across the interface.

In order to couple the temperature and concentration distribution, it is necessary to introduce an additional boundary condition using the third assumption; that is:

$$\left\{\begin{array}{l}\text{The temperature-concentration relation may}\\ \text{be expressed by the equilibrium condition}\end{array}\right\} \tag{34}$$

with

$$\left.\begin{aligned} C'_{is} &= f'_i(T_s, P''_\infty)\\ C''_{is} &= f''_i(T_s, P''_\infty)\end{aligned}\right\}$$

C. Solutions

Chapter 11 of Ref. 22 indicates that the similarity variables

$$\left.\begin{aligned} \eta' &= \frac{x}{2\sqrt{\alpha' t}}\\ \eta'' &= \frac{x}{2\sqrt{\alpha'' t}}\end{aligned}\right\} \tag{35}$$

may be used to obtain an exact solution to Eqs. (25) and (26). Introducing these variables and u" as expressed by Eq. (32) into Eqs. (26) and (26) yields

$$\frac{d^2T''}{d\eta''^2} + 2\left[\eta'' + \frac{\rho' - \rho''}{\rho''}\lambda\sqrt{\frac{\alpha'}{\alpha''}}\right]\frac{dT''}{d\eta''} = 0 \tag{36}$$

$$\frac{d^2T'}{d\eta'^2} + 2\eta'\frac{dT'}{d\eta'} = 0 \tag{37}$$

The general solutions in dimensionless form for T" and T' which satisfy Eqs. (36) and (37) and the appropriate initial and boundary conditions represented by Eqs. (33a), (33b) and (33c) are

$$\frac{T' - T'_\infty}{T''_\infty - T'_\infty} = A'(\lambda)\left[1 + \operatorname{erf}\frac{x}{2\sqrt{\alpha' t}}\right] \tag{38}$$

$$\frac{T''_\infty - T'}{T''_\infty - T'_\infty} = A''(\lambda)\operatorname{erfc}\left[\frac{x}{2\sqrt{\alpha'' t}} + \frac{\lambda(\rho' - \rho'')}{\rho''}\sqrt{\frac{\alpha'}{\alpha''}}\right] \tag{39}$$

The integration constants A_1 and A_2 are determined by Eqs. 33d and 33e as

$$A'(\lambda) = \frac{\delta_T \lambda \operatorname{erfc}(\gamma_T \lambda) + \sigma_T e^{-\lambda^2 \gamma_T^2}}{e^{-\lambda^2}\operatorname{erfc}(\gamma_T \lambda) + \sigma_T\, e^{-\lambda^2 \gamma_T^2}(1 + \operatorname{erf}\lambda)} \tag{40}$$

$$A''(\lambda) = \frac{e^{-\lambda^2} - \delta_T \lambda(1 + \operatorname{erf}\lambda)}{e^{-\lambda^2}\operatorname{erfc}(\gamma_T \lambda) + \sigma_T e^{-\lambda^2 \gamma_T^2}(1 + \operatorname{erf}\lambda)} \tag{41}$$

where

$$\delta_T = \frac{\sqrt{\pi} h_{fg}}{C_p'(T''_\infty - T'_\infty)} \tag{42a}$$

$$\gamma_T = \frac{\rho'}{\rho''}\sqrt{\frac{\alpha'}{\alpha''}} \tag{42b}$$

$$\sigma_T = \sqrt{\frac{(\rho C_p k)''}{(\rho C_p k)'}} \tag{42c}$$

The interfacial temperature T_s at $x = 2\lambda\sqrt{\alpha' t}$ is

$$\frac{T_s - T'_\infty}{T''_\infty - T'_\infty} = A'(\lambda)\,(1 + \operatorname{erf}\lambda) \tag{43}$$

Similarly, the similarity variables

$$\left.\begin{aligned} \eta_i' &= \frac{x}{2\sqrt{\mathfrak{D}_i' t}} \\ \eta_i'' &= \frac{x}{2\sqrt{\mathfrak{D}_i'' t}} \end{aligned}\right\} \tag{44}$$

and u" as expressed by Eq. (32) may be introduced into Eqs. (27) and (28), yielding

$$\frac{d^2C_i''}{d\eta_i''^2} + 2\left[\eta_i'' + \frac{\rho' - \rho''}{\rho''}\lambda\sqrt{\frac{\alpha'}{\mathfrak{D}_i'}}\right]\frac{dC_i''}{d\eta_i''} = 0 \tag{45}$$

$$\frac{d^2C_i'}{d\eta_i'^2} + 2\eta_i'\frac{dC_i'}{d\eta_i'} = 0 \tag{46}$$

The general solutions in dimensionless form for C_i' and C_i'' of the i-th component are obtained as follows; they satisfy Eqs. (45) and (46) and the appropriate initial and boundary conditions, Eqs. (33f) through (33j):

$$\frac{C_{i\infty}'' - C_i''}{C_{i\infty}'' - C_{i\infty}'} = D_i(\lambda)\operatorname{erfc}\left[\frac{x}{2\sqrt{\mathfrak{D}_i't}} + \frac{\lambda(\rho' - \rho'')}{\rho''}\sqrt{\frac{\alpha'}{\mathfrak{D}_i''}}\right] \tag{47}$$

$$\frac{C_i' - C_{i\infty}'}{C_{i\infty}'' - C_{i\infty}'} = B_i(\lambda)\left(1 + \operatorname{erf}\frac{x}{2\sqrt{\mathfrak{D}_i't}}\right) \tag{48}$$

where

$$B_i(\lambda) = \frac{C_{is}' - C_{i\infty}'}{(C_{i\infty}'' - C_{i\infty}')\left(1 + \operatorname{erf}\lambda\sqrt{\frac{\alpha'}{\mathfrak{D}_i}}\right)} \tag{49}$$

$$D_i(\lambda) = \frac{C_{is}'' - C_{i\infty}''}{(C_{i\infty}'' - C_{i\infty}')\operatorname{erfc}\left[\lambda\sqrt{\frac{\alpha'}{\mathfrak{D}_i''}} + \frac{\lambda(\rho' - \rho'')}{\rho''}\sqrt{\frac{\alpha'}{\mathfrak{D}_i''}}\right]} \tag{50}$$

The relationship between λ, C_{is}'', and C_{is}' is

$$\frac{(C_{is}' - C_{i\infty}')e^{-\left(\lambda\sqrt{\frac{\alpha'}{\mathfrak{D}_i'}}\right)^2}}{1 + \operatorname{erf}\lambda\sqrt{\frac{\alpha'}{\mathfrak{D}_i'}}} - \frac{(C_{is}'' - C_{i\infty}'')\sqrt{\frac{\mathfrak{D}_i''}{\mathfrak{D}_i'}}\,e^{-\left(\lambda\frac{\rho'}{\rho''}\sqrt{\frac{\alpha'}{\mathfrak{D}_i''}}\right)^2}}{\operatorname{erfc}\left(\lambda\frac{\rho'}{\rho''}\sqrt{\frac{\alpha'}{\mathfrak{D}_i''}}\right)}$$

$$= \sqrt{\pi}\rho'\lambda\sqrt{\frac{\alpha'}{\mathfrak{D}_i'}}\left(\frac{C_{is}''}{\rho''} - \frac{C_{is}'}{\rho'}\right) \tag{51}$$

The interfacial concentration of the i-th components at $x = 2\lambda\sqrt{\alpha' t}$ is

$$\left.\begin{aligned} \frac{C''_{i\infty} - C''_{is}}{C''_{i\infty} - C'_{i\infty}} &= \beta_i(\lambda)\ \mathrm{erfc}\left(\lambda \frac{\rho'}{\rho''}\sqrt{\frac{\alpha'}{\beta''_i}}\right) \\ \frac{C'_{is} - C'_{i\infty}}{C''_{i\infty} - C'_{i\infty}} &= B_i(\lambda)\left(1 + \mathrm{erf}\ \lambda\sqrt{\frac{\alpha'}{\beta'_i}}\right) \end{aligned}\right\} \qquad (52)$$

λ can be obtained by coupling T_s as expressed in Eq. (43) and C_{is} as expressed in Eq. (52) according to the relationship expressed by Eq. (34), which gives the constant characterizing the interfacial movement.

The total interfacial mass transfer N_T is

$$\begin{aligned} N_T &= \rho' \int_0^t \frac{dX}{dt}\, dt = \rho' X(t) \\ &= 2\lambda\rho'\sqrt{\alpha' t} \end{aligned} \qquad (53)$$

The equations for interfacial heat transfer, which may be written as $q/A = -k\,(\partial T/\partial x)$, are obtained as follows for the liquid and gas regions:

$$\frac{(q/A)'}{k'(T''_\infty - T'_\infty)} = \frac{A'(\lambda)}{\sqrt{\pi\alpha' t}}\, e^{-\lambda^2} \qquad (54)$$

$$\frac{(q/A)''}{k''(T''_\infty - T'_\infty)} = \frac{A''(\lambda)}{\sqrt{\pi\alpha'' t}}\, e^{-(\gamma_T\lambda)^2} \qquad (55)$$

D. Special Cases

1. ZERO CONDENSATION RATE ($\lambda = 0$)

This particularly interesting special case, $\lambda = 0$, is the case separating condensation from evaporation. For this case, Eqs. (33) and (39) reduce to

$$\frac{T' - T'_\infty}{T''_\infty - T'_\infty} = A'(0)\left(1 + \operatorname{erf} \frac{x}{2\sqrt{\alpha' t}}\right) \tag{56}$$

$$\frac{T''_\infty - T''}{T''_\infty - T'_\infty} = A''(0) \operatorname{erfc} \frac{x}{2\sqrt{\alpha'' t}} \tag{57}$$

where

$$A'(0) = \frac{1}{1 + \sqrt{\frac{(\rho C_p k)'}{(\rho C_p k)''}}} \tag{58}$$

$$A''(0) = \frac{1}{1 + \sqrt{\frac{(\rho C_p k)''}{(\rho C_p k)'}}} \tag{59}$$

The interfacial temperature as obtained from Eq. (43) is

$$\frac{T_s - T'_\infty}{T''_\infty - T'_\infty} = A'(0) \tag{60}$$

For concentration distribution, Eqs. (47) and (48) reduce to

$$\frac{C''_{i\infty} - C''_i}{C''_{i\infty} - C'_{i\infty}} = D_i(0) \operatorname{erfc} \frac{x}{2\sqrt{\mathcal{D}''_i t}} \tag{61}$$

$$\frac{C'_i - C'_{i\infty}}{C''_{i\infty} - C'_{i\infty}} = B_i(0)\left(1 + \operatorname{erf} \frac{x}{2\sqrt{\mathcal{D}'_i t}}\right) \tag{62}$$

where

$$B_i(0) = \frac{C'_{is} - C'_{i\infty}}{C''_{i\infty} - C'_{i\infty}} \tag{63}$$

$$D_i(0) = \frac{C''_{is} - C''_{i\infty}}{C''_{i\infty} - C'_{i\infty}} \tag{64}$$

The interfacial concentration of the i-th component as obtained from Eq. (52) is

$$\left.\begin{aligned} \frac{C''_{i\infty} - C''_{is}}{C''_{i\infty} - C'_{i\infty}} &= D_i(0) \\ \frac{C'_{is} - C'_{i\infty}}{C''_{i\infty} - C'_{i\infty}} &= B_i(0) \end{aligned}\right\} \tag{65}$$

The combination of Eqs. (54), (55), (58), and (59) gives

$$(q/A)' = (q/A)'' = \frac{T''_\infty - T'_\infty}{\sqrt{\pi t}\left[\frac{1}{\sqrt{(\rho C_p k)'}} + \frac{1}{\sqrt{(\rho C_p k)''}}\right]} \tag{66}$$

Equation (66) indicates that in this special case the heat transferred toward the interface in one phase equals the heat transferred away from the interface in the other phase.

2. CASE OF $(\rho C_p k)' \gg (\rho C_p k)''$

For a large number of practical applications, the magnitude of

$$\frac{(\rho C_p k)''}{(\rho C_p k)'}$$

is small in comparison with unity. Therefore Eq. (40) may be written as

$$A'(0) = \frac{\sqrt{\pi} h_{fg} \lambda}{C'_p (T''_\infty - T'_\infty) e^{-\lambda^2}} \tag{67}$$

For this case λ may be found by the combination of Eqs. (43) and (67). In addition to a small

$$\frac{(\rho C_p k)''}{(\rho C_p k)'},$$

if λ is sufficiently small such that $e^{-\lambda^2}$ and $(1 + \operatorname{erf} \lambda)$ may be approximated by unity, then λ may be obtained by the substitution of Eq. (67) into Eq. (43) as

$$\lambda = \frac{C_p'(T_s - T'_\infty)}{\sqrt{\pi} h_{fg}} \tag{68}$$

This expression is in agreement with λ obtained for the same case by the source theory, which will be presented in detail in the next progress report. The approximation as expressed by Eq. (68) is good especially for small values of the temperature difference $T''_\infty - T'_\infty$. If $T''_\infty - T'_\infty$ is considerably large, the interfacial movement will be rapid and the approximation given by Eq. (68) will deviate more from the exact solution. As indicated by Eq. (68), $\lambda = 0$ when the interfacial temperature T_s is equal to the liquid temperature T'_∞ or when

$$\frac{C_{p'}}{h_{fg}} \cong 0 \quad .$$

The substitution of Eq. (68) into Eq. 53 yields

$$N_T = \frac{2\rho' C_p' (T_s - T'_\infty)}{\sqrt{\pi} h_{fg}} \sqrt{\alpha' t} \tag{69}$$

which is a linear form for the interfacial mass transfer rate.

The analytical expressions derived in Section C will now be used to carry out some illustrative applications to one- and two-component systems.

3. ONE-COMPONENT SYSTEM

The governing differential equations for this case are Eqs. (25) and (26). The appropriate initial and boundary conditions are expressed by Eqs. (33a) through (33e). Equations (38) and (39) give the transient temperature distribution in the liquid and gas regions respectively. λ as obtained from Eq. (43), with T_s assumed as the saturation temperature corresponding to P''_∞ is substituted into Eqs. (52), (54), and (55) to determine the total interfacial mass transfer and the interfacial heat transfer for the liquid and gas regions.

4. BINARY COMPONENT SYSTEM (Components 1 and 2)

The governing differential equations are Eqs. (25) and (26) for temperature distribution and Eqs. (27) and (28) for concentration distribution. The appropriate initial and boundary conditions are expressed by Eqs. (33a) through (33j) with i = 1. The transient temperature and concentration distributions in both liquid and gas regions are expressed by Eqs. (38), (39), (47), and (48) with i = 1. Equations (43) and (52) respectively represent the temperature and concentration at the interface. λ in Eqs. (38), (39), (43), (47), (48), and (52) has to be determined by the equilibrium conditions between the interfacial temperature and concentration; that is T_s, C'_s, and C''_s as expressed respectively by Eqs. (43) and (52) must be coupled by the equilibrium conditions at the interface. For example,

the T_s - C_s relationship may be approximated linearly as follows, for a system consisting of one component in gas phase and two components in liquid phase.

$$C'_{is} - C'_{i\infty} = \left(\frac{\partial C'_i}{\partial T}\right)_p (T_s - T'_{\infty,sat}) \tag{70}$$

or

$$C'_{is} - C'_{i\infty} = \left(\frac{\partial C'_j}{\partial T}\right)_p (T'_{\infty,sat} - T_s) \tag{71}$$

at $x = X(t)$. Then λ is determined by Eqs. (56) and (57), into which Eqs. (43) and (52) are substituted. That is,

$$B_1(\lambda)(C''_{i\infty} - C'_{i\infty})\left(1 + \operatorname{erf} \lambda \sqrt{\frac{\alpha'}{\beta'}}\right)$$

$$= \left(\frac{\partial C_i}{\partial T}\right)_p [T'_\infty - T'_{\infty,sat} + A_1(\lambda)(T''_\infty - T'_\infty)(1 + \operatorname{erf} \lambda)] \tag{72}$$

E. Approximate Solutions

Approximate solutions obtained by the uses of the source theory and the integral method will be presented in the next progress report. A comparison between the exact and approximate solutions will also be given.

REFERENCES

1. Clark, J. A., H. Merte and V. S. Arpaci, et al, Pressurization of Liquid Oxygen Containers, Final Report, ORA Project 03583, Department of the Army Contract No. DA-20-018-506-ORD-254, University of Michigan, March, 1961.

2. Clark, J. A., H. Merte, V. S. Arpaci, et al. Pressurization of Liquid Oxygen Containers, Progress Report No. 2, ORA Report 04268-2-P, NASA Contract No. NAS-8-825, The University of Michigan, November 1961.

3. Clark, J. A., H. Merte, V. S. Arpaci, et al, Pressurization of Liquid Oxygen Containers, Progress Report No. 4, ORA Report 04268-4-P, NASA Contract No. NAS-8-825, The University of Michigan, July 1962.

4. Arpaci, V. S., and J. A. Clark, "Dynamic Response of Fluid and Wall Temperatures During Pressurized-Discharge for Simultaneous, Time-Dependent Inlet Gas Temperature, Ambient Temperature and/or Ambient Heat Flux," Advances in Cryogenic Engineering, Vol. 7, Plenum Press, 1962.

5. Frederking, T.H.K., and J. A. Clark, "Film Boiling of Liquid Nitrogen from a Sphere," 1962 Cryogenic Engineering Conference, Los Angeles, California, to be published in Advances in Cryogenic Engineering, Vol. 8, 1963.

6. Bromley, L. A., "Heat Transfer in Stable Film Boiling," Chem. Eng. Prog., 46, 221 (1950).

7. Berenson, P. J., "Film-Boiling Heat Transfer from a Horizontal Surface," Trans. ASME, J. Heat Transfer, 83c No. 3, 351, 1961.

8. Chang, Y. and N. W. Snyder, "Heat Transfer in Saturated Boiling," Preprint 104 presented at Third National Heat Transfer Conference, ASME-AIChE August 1959.

9. Merte, H., Jr., and J. A. Clark, "Pool Boiling in An Accelerating System," Journal of Heat Transfer, August 1961.

10. Clark, J. A., H. Merte, V. S. Arpaci, et al, Pressurization of Liquid Oxygen Containers, Progress Report No. 3, ORA Report 04268-3-P, NASA Contract No. NAS-8-825, The University of Michigan, March 1962.

11. "Recent Advances in Heat and Mass Transfer," Edited by J. P. Hartnett, McGraw-Hill Book Company, Inc., New York 1961, p. 302.

12. Higbie, R., "The Rate of Absorption of a Pure Gas into a Still Liquid During Short Periods of Exposure," Trans. AIChE, Vol. 31 (1935), pp 365-389.

13. Rayleigh, Lord, Phil. Mag., 34, (1917-8), pp. 94.

14. Plesset, M. S., "The Dynamics of Cavitation Bubbles," J. of Appl. Mech., 16, 1949.

15. Plesset, M. S. and S. A. Zwick, "The Growth of Vapor Bubbles in Super-heated Liquids," J. of Appl. Phys., 25, 1954, pp 493-500.

16. Forster, H. K. and N. Zuber, "Growth of a Vapor Bubble in a Superheated Liquid," J. of Appl. Phys., 25, 1954, pp 474.

17. Chambre, P. L., "On the Dynamics of Phase Growth," Q. J. of Mech. Appl. Math., 9, 1956, pp 224.

18. L. E. Scriven, "On the Dynamics of Phase Growth," Chem. Eng. Science, 10, 1959, pp 1-13.

19. Yang, W. J. and J. A. Clark, "Dynamics of Bubble Growth and Collapse," Manuscript in Preparation, 1962.

20. Thomas, P. D. and F. H. Morse, "Analytic Solution for the Phase Change in a Suddenly Pressurized Liquid-Vapor System," Advances in Cryogenic Engineering, 8, 1962.

21. E. L. Knuth, "Evaporations and Condensations in One-Component Systems," paper to be published in Amer. Rocket Society, 1962.

22. Carslaw, H. S. and J. C. Jaeger, Conduction of Heat in Solids Oxford University Press, 2nd ed. 1959.

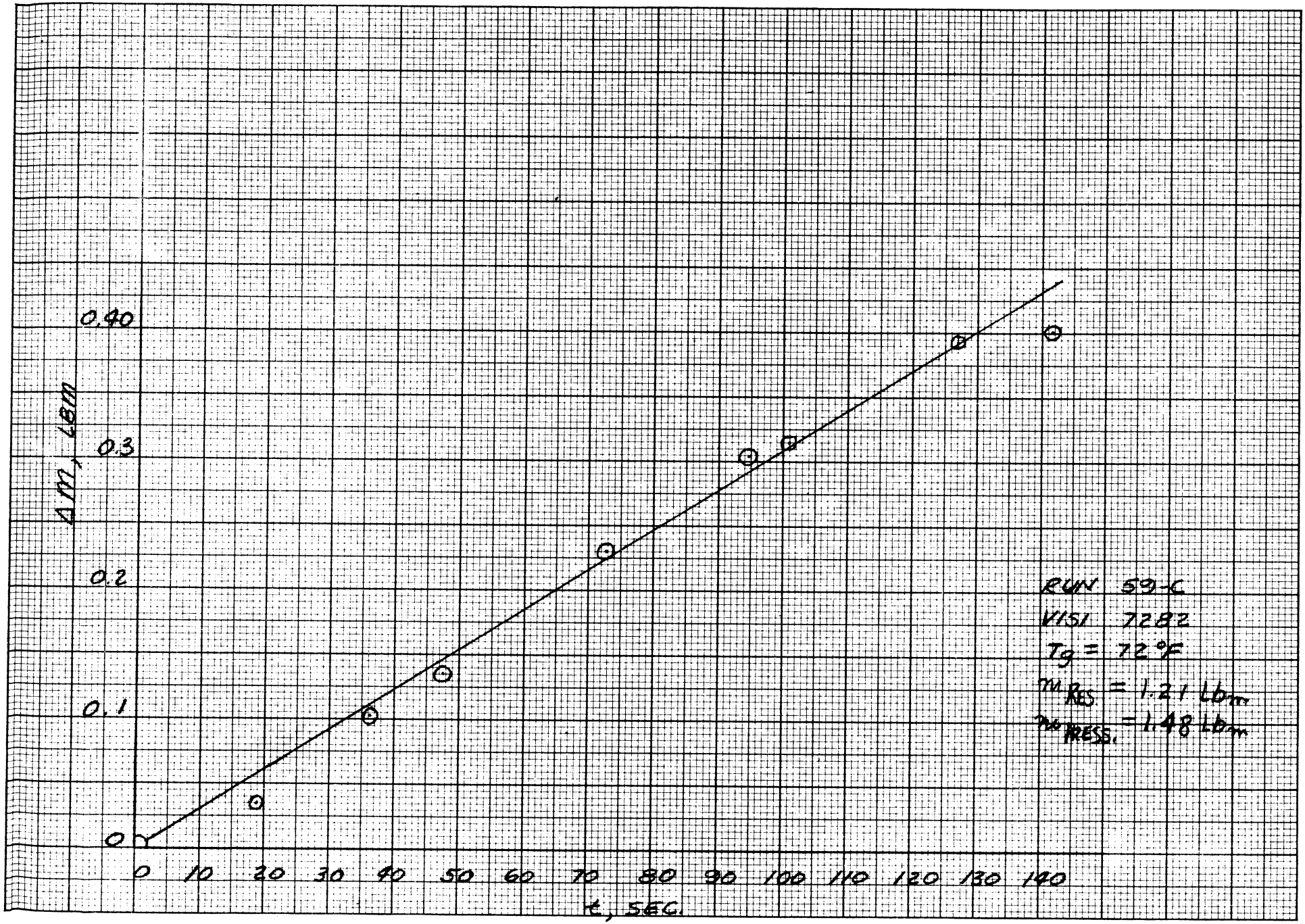

FIGURE 1. MASS CONDENSED DURING DISCHARGE. $T_g = 72°F$

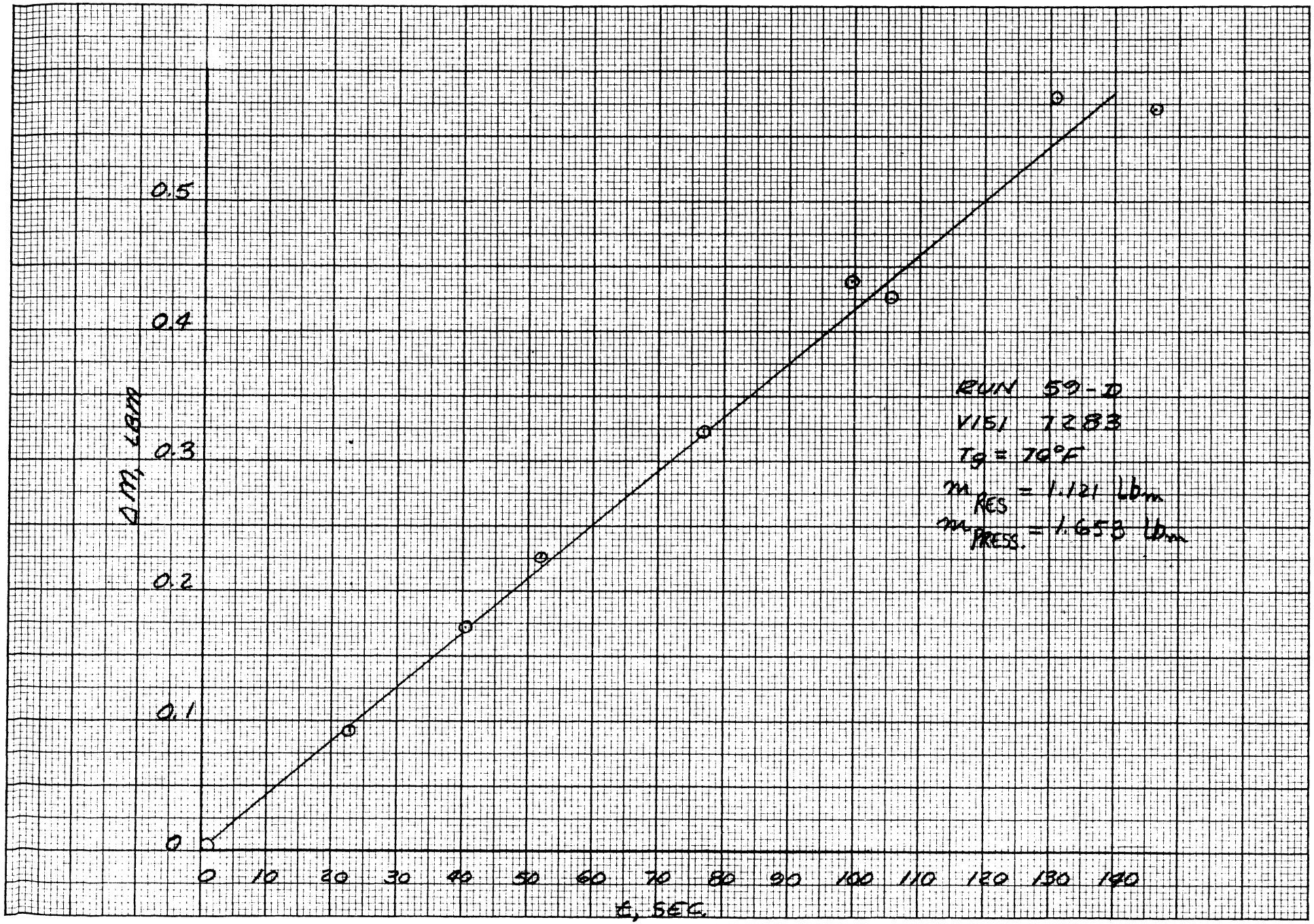

FIGURE 2. MASS CONDENSED DURING DISCHARGE. $T_g = 70°F$

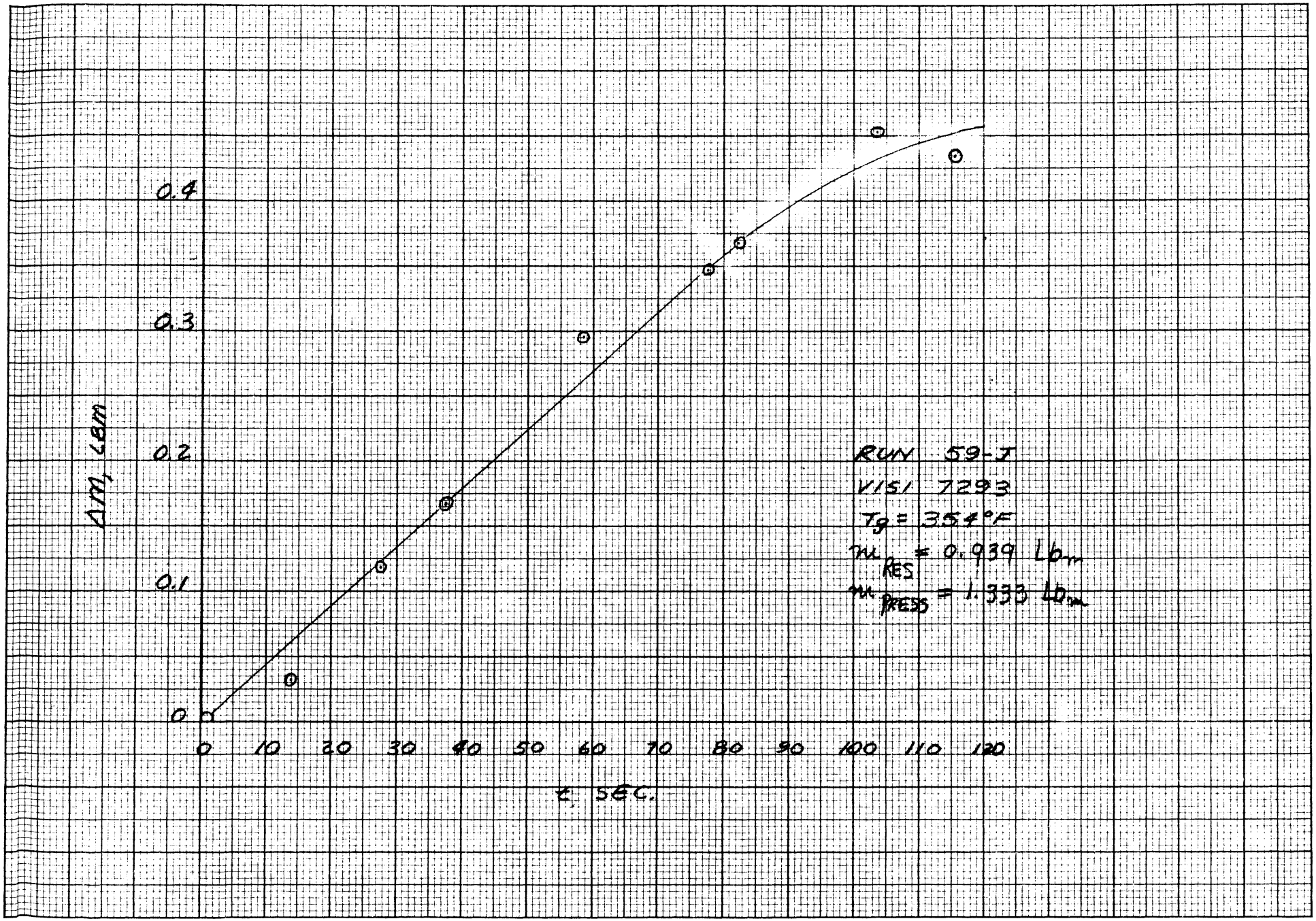

FIGURE 3. MASS CONDENSED DURING DISCHARGE. T_g = 354 °F

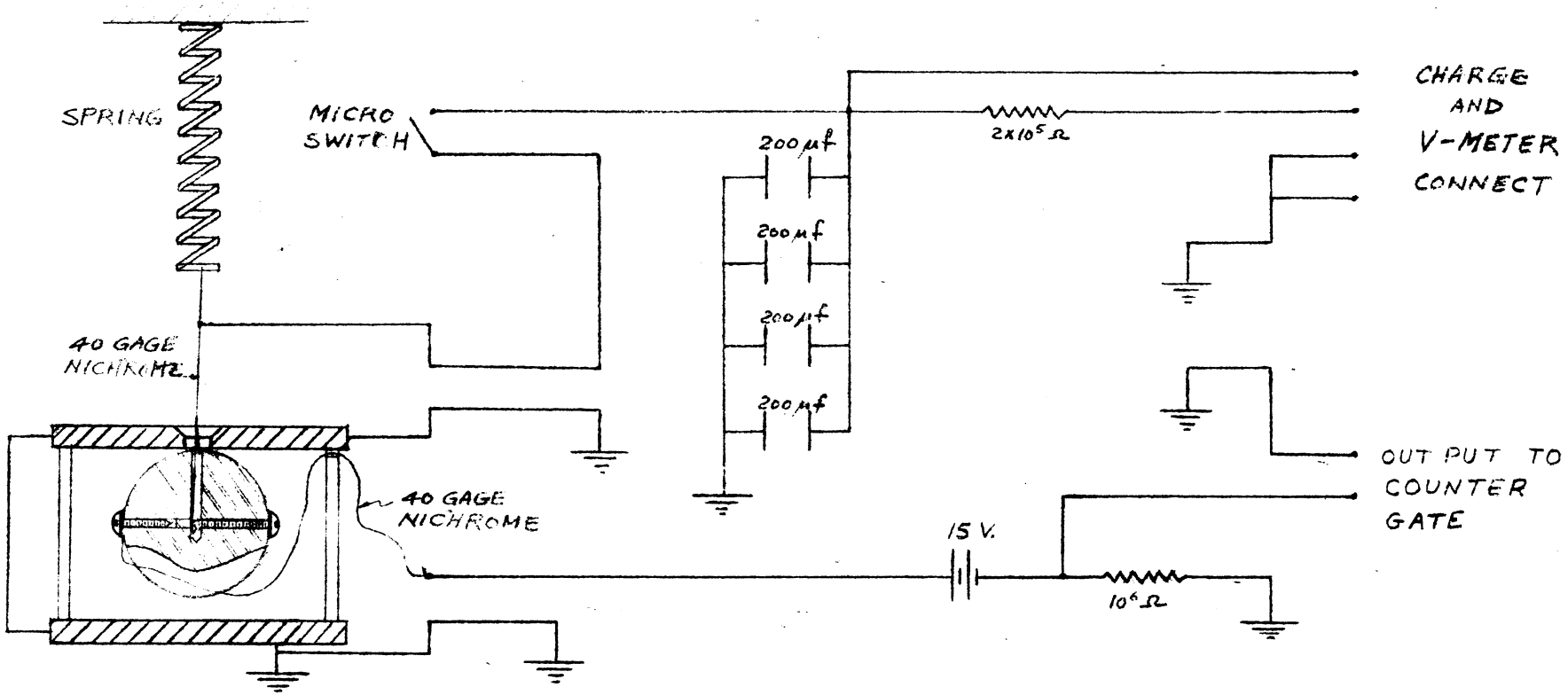

FIGURE 4. BALL-DROP ACCELEROMETER SCHEMATIC DIAGRAM

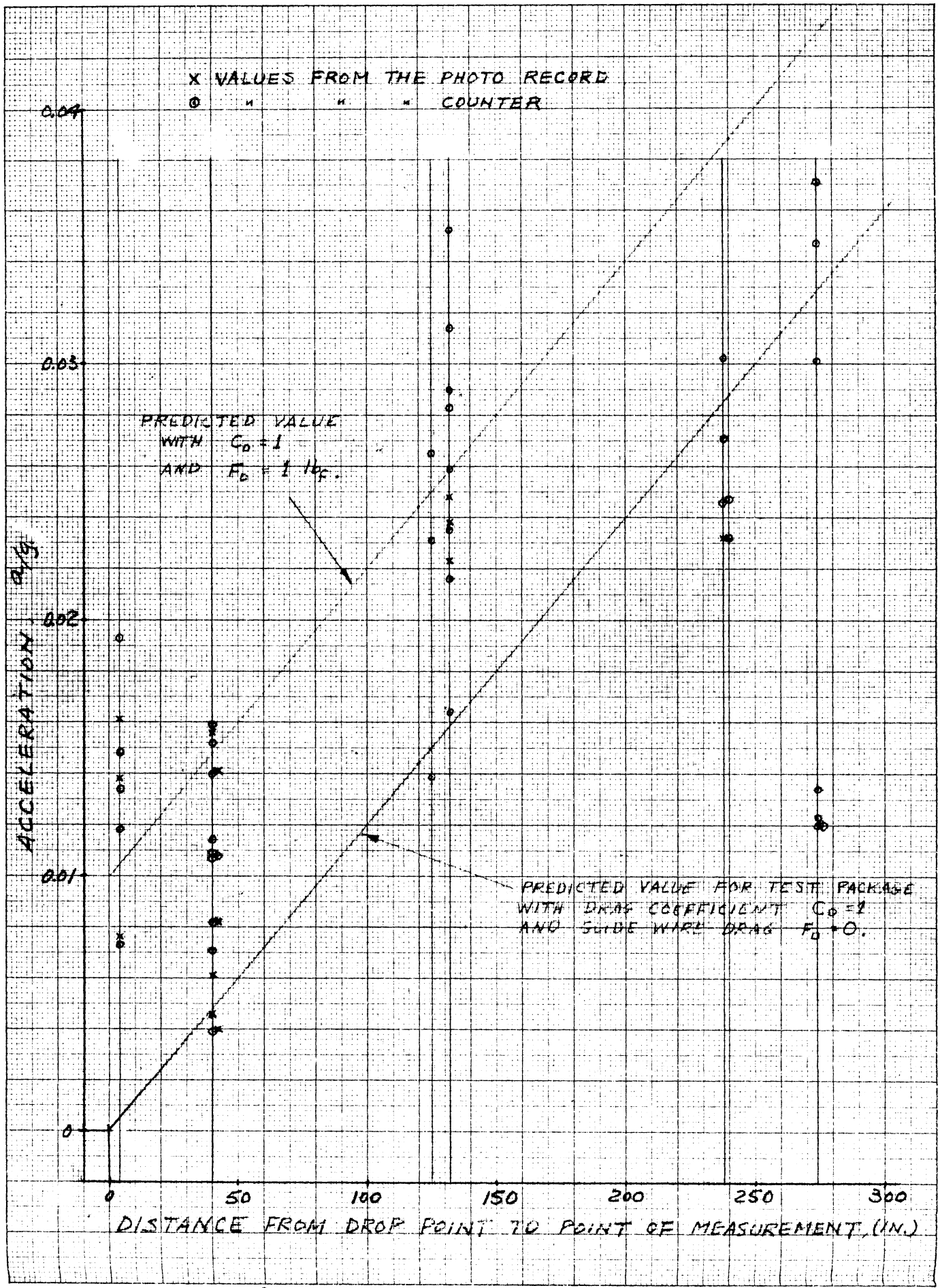

FIGURE 5. DROP-BALL ACCELEROMETER MEASUREMENTS WITH TEST PACKAGE UNDER FREE FALL.

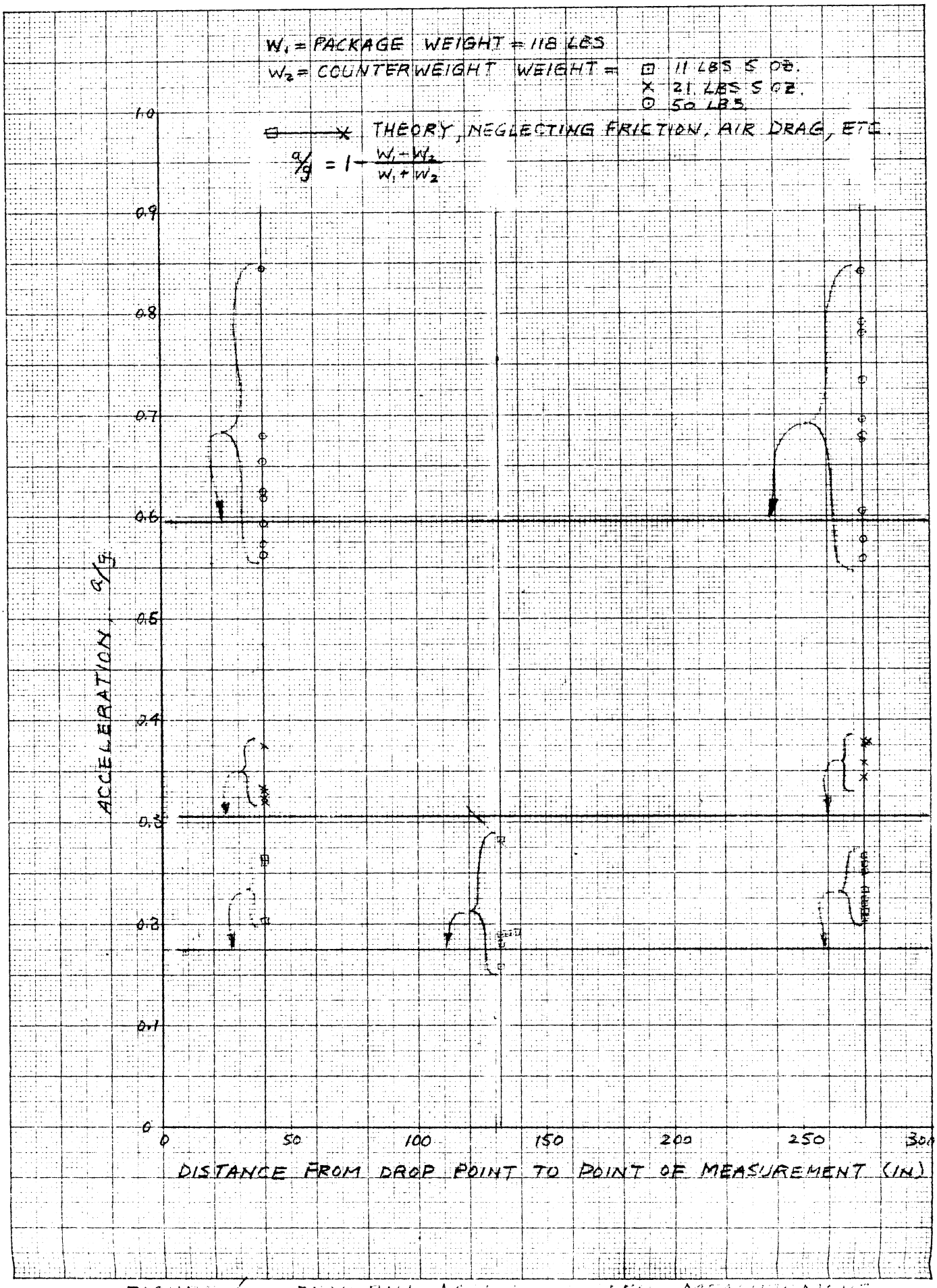

FIGURE 6. DROP-BALL ACCELEROMETER MEASUREMENTS WITH TEST PACKAGE UNDER COUNTERWEIGHT FALL.

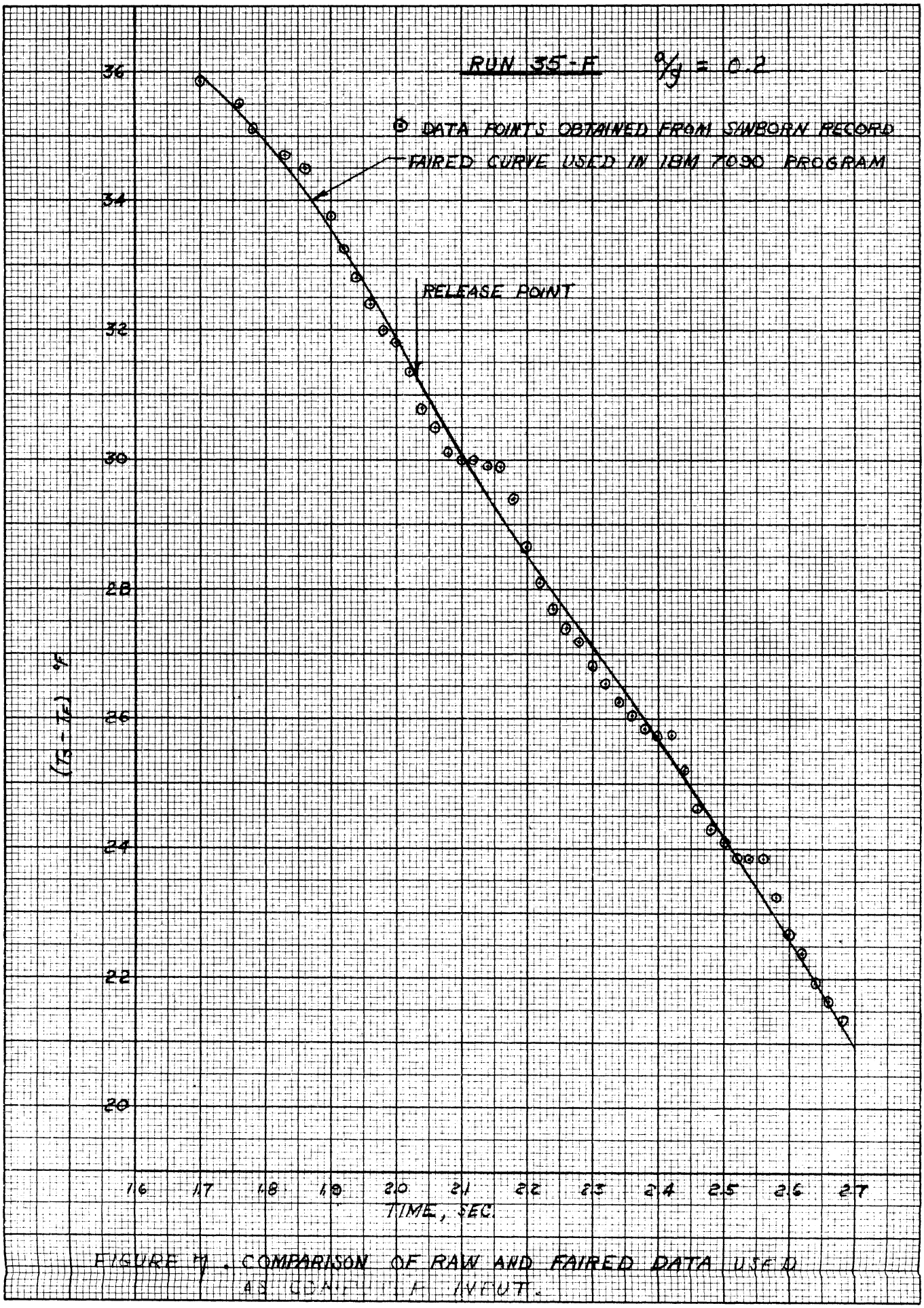

FIGURE M. COMPARISON OF RAW AND FAIRED DATA USED AS GEAR A INPUT.

2 X 3 CYCLES

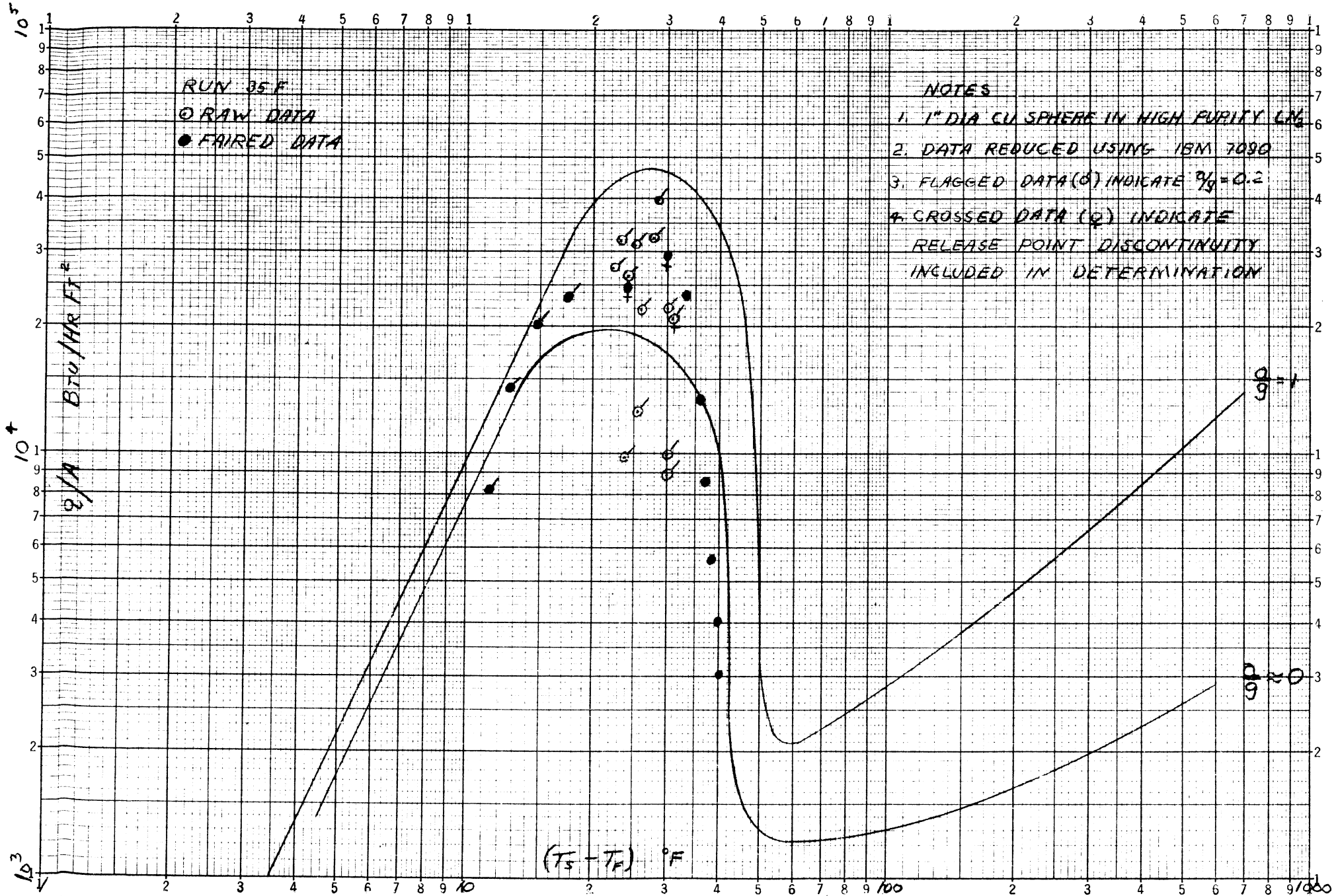

FIGURE 8. COMPARISON OF IBM 7090 RESULTS FOR RAW & FAIRED DATA INPUTS

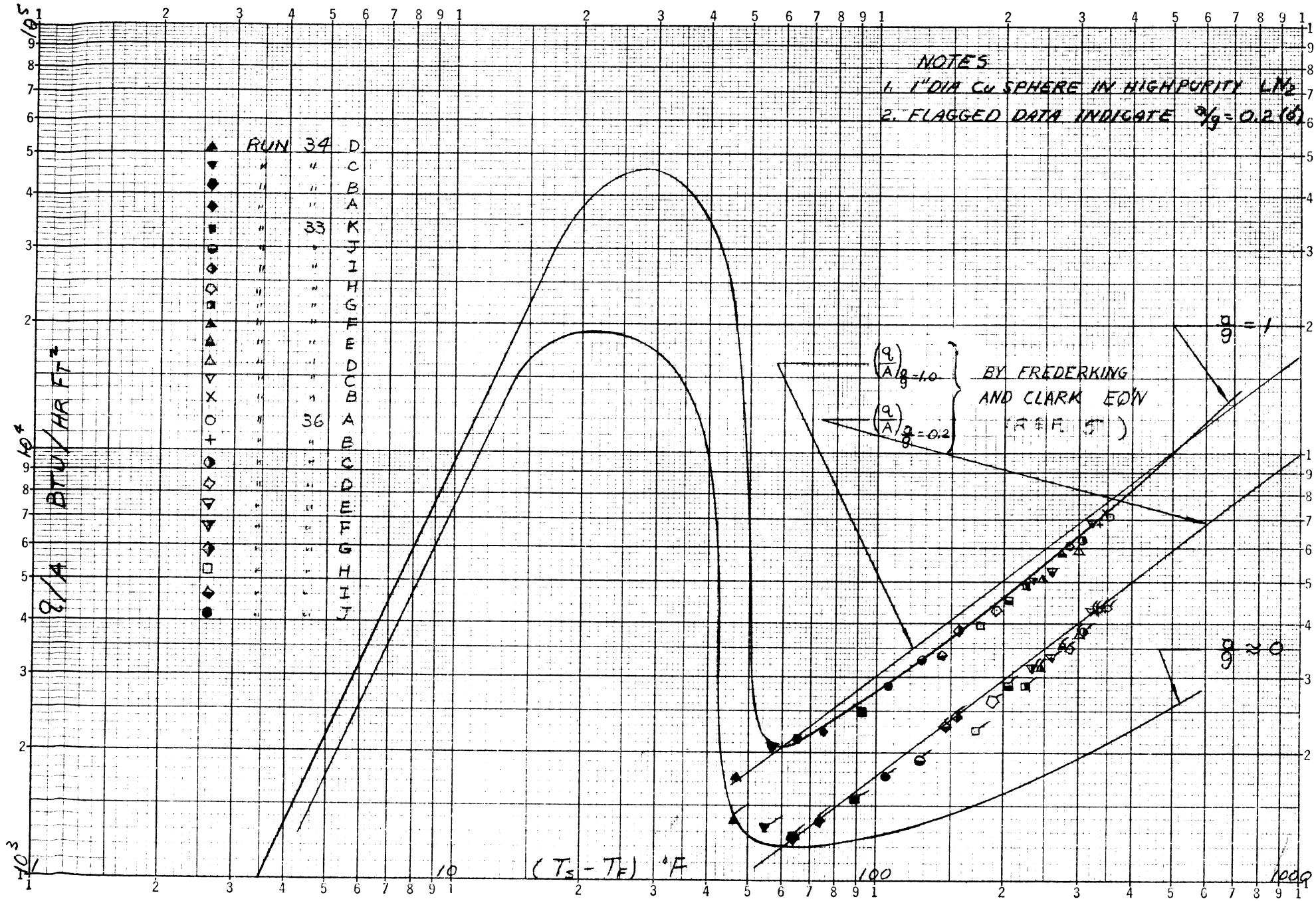

FIGURE 9. BOILING HEAT TRANSFER DATA IN THE FILM REGION FOR $q/g = 1$ & 0.2

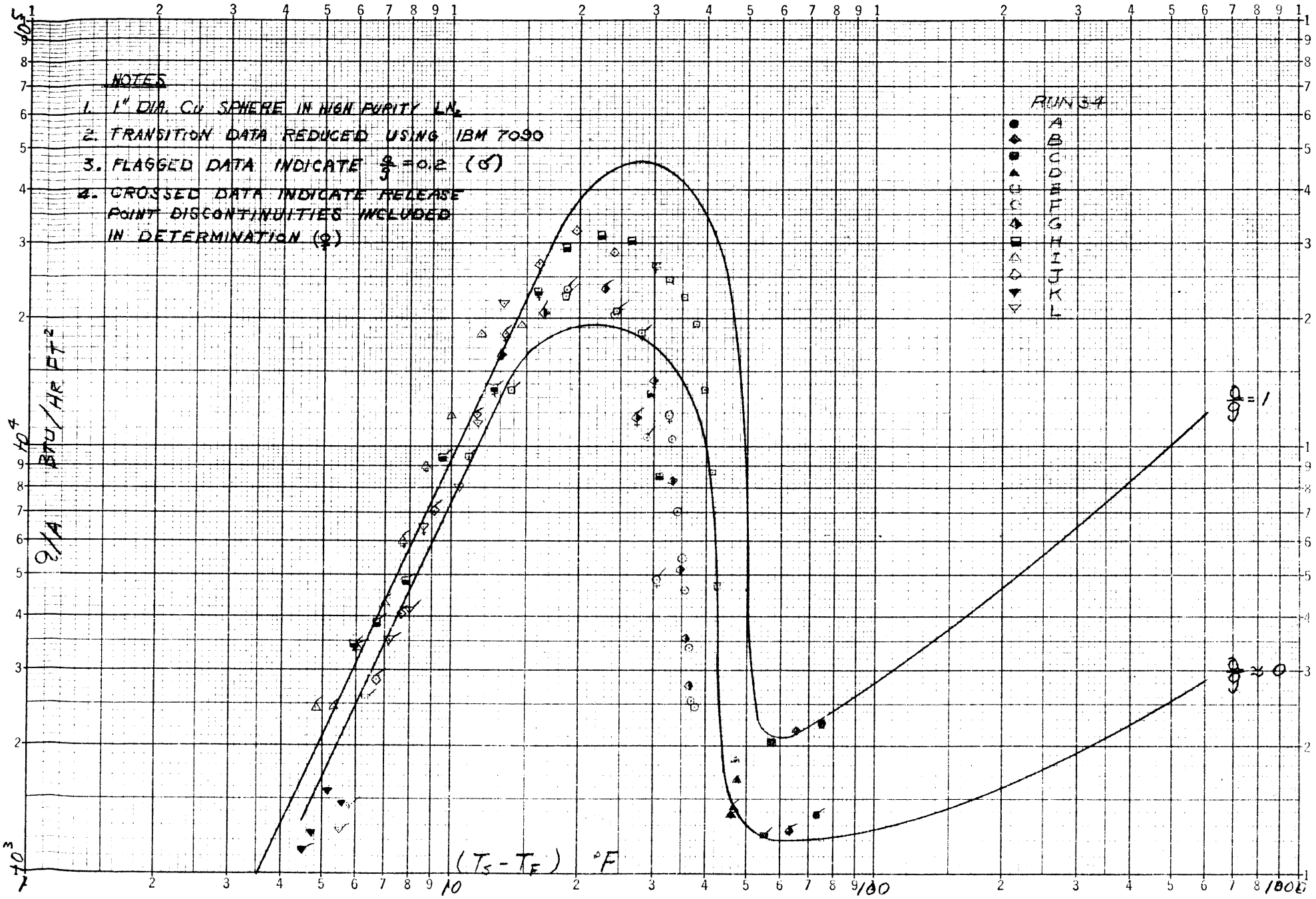

FIGURE 10. BOILING HEAT TRANSFER DATA IN THE TRANSITION REGION FOR $\sigma/g = 1 \pm 0.2$

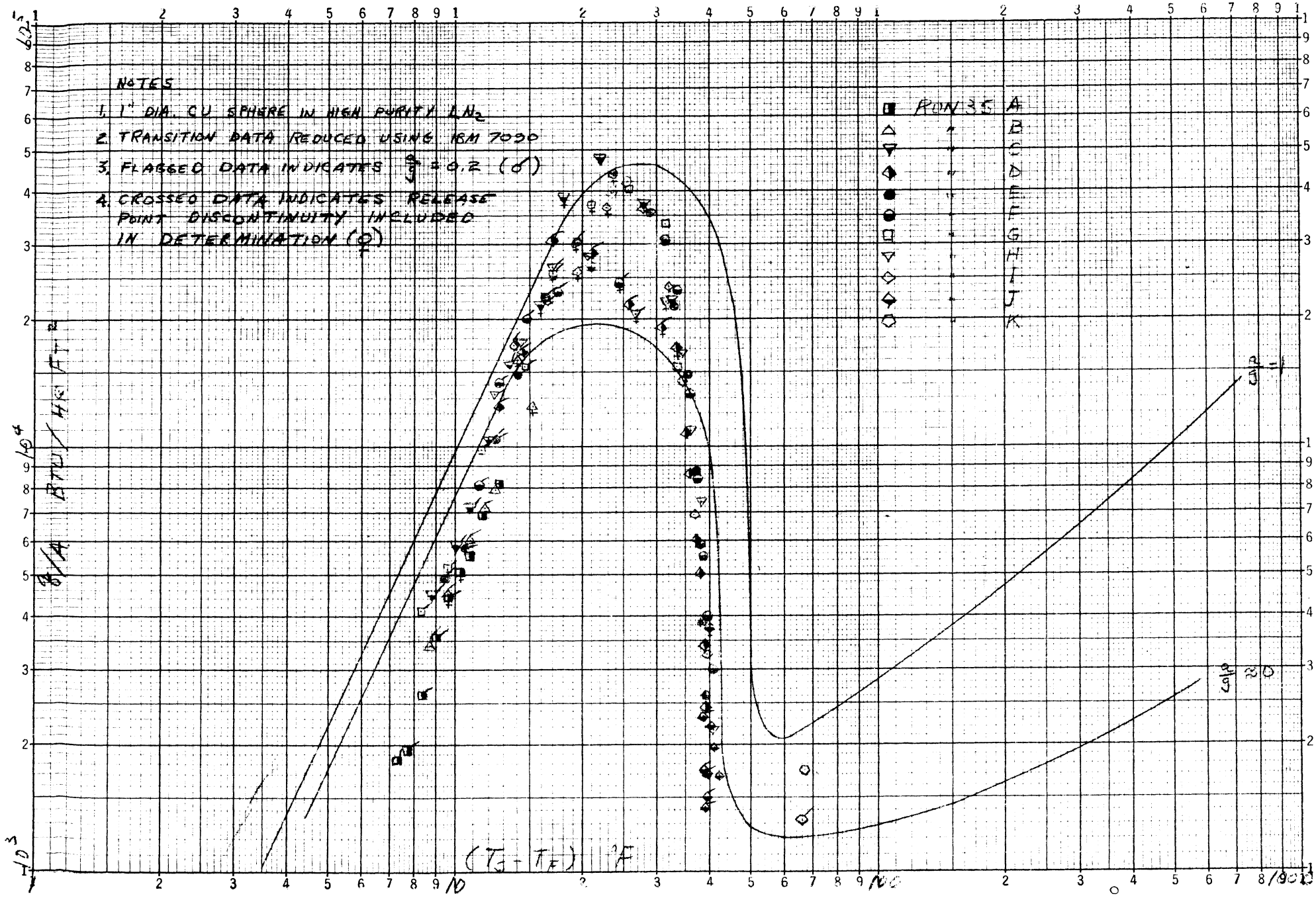

FIGURE 11. BOILING HEAT TRANSFER DATA IN THE TRANSITION REGION FOR $\frac{\rho_v}{\rho_l} = 1$ & 0.2

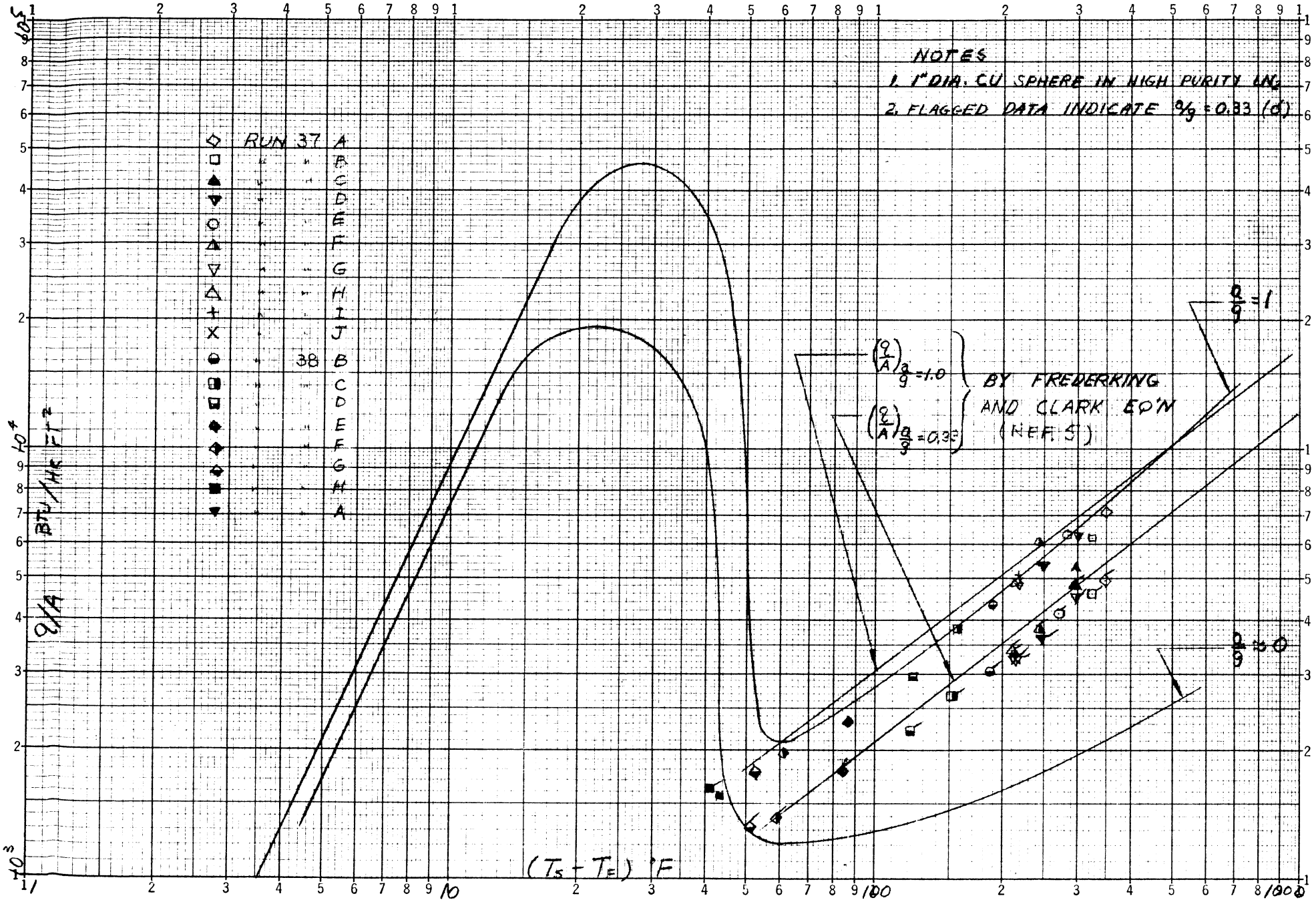

FIGURE 12. BOILING HEAT TRANSFER DATA IN THE FILM BOILING REGION FOR q/g = 1.0 & 0.33

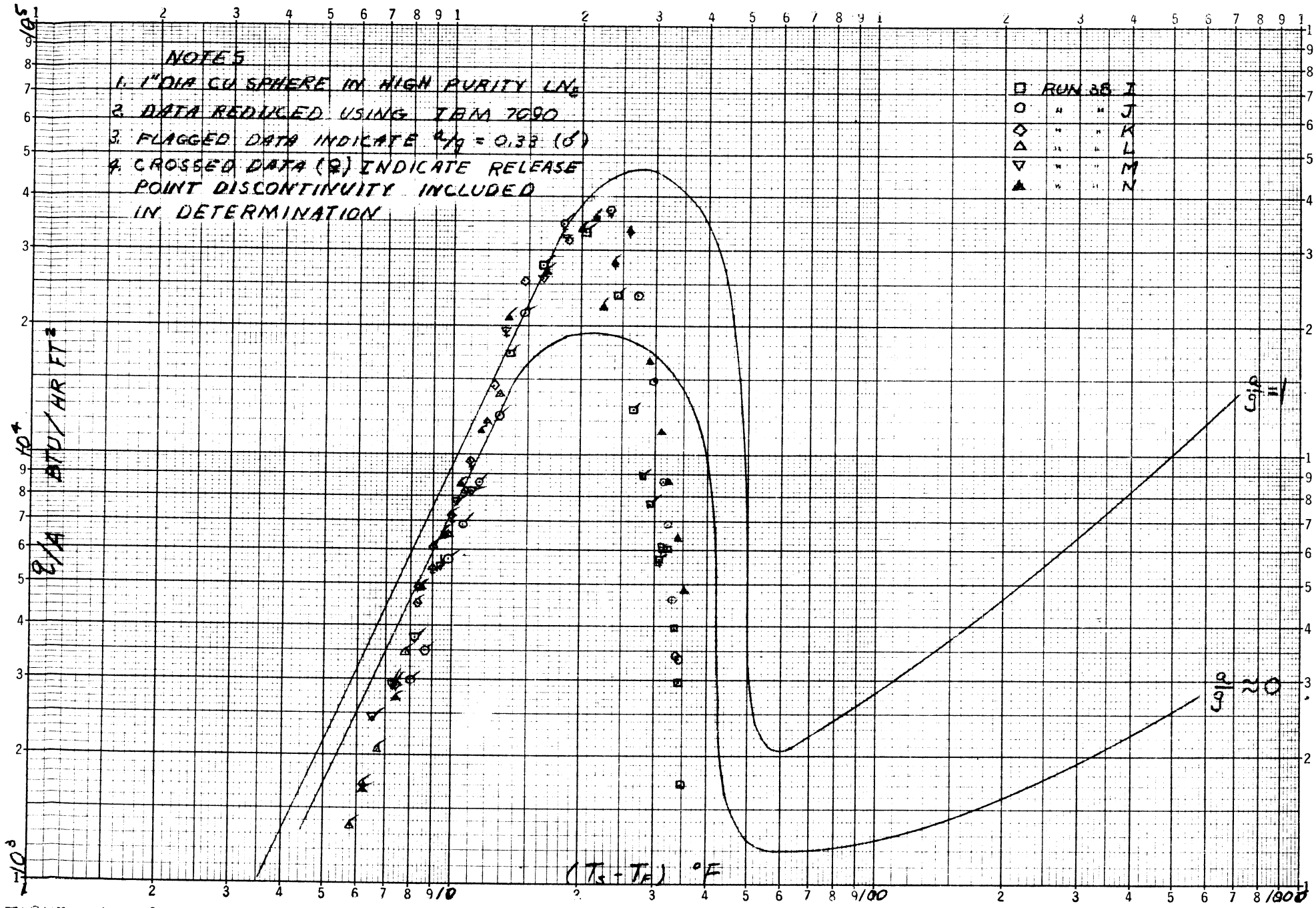

FIGURE 13. BOILING HEAT TRANSFER DATA IN THE TRANSITION REGION FOR $a/g = 1.0$ & 0.33

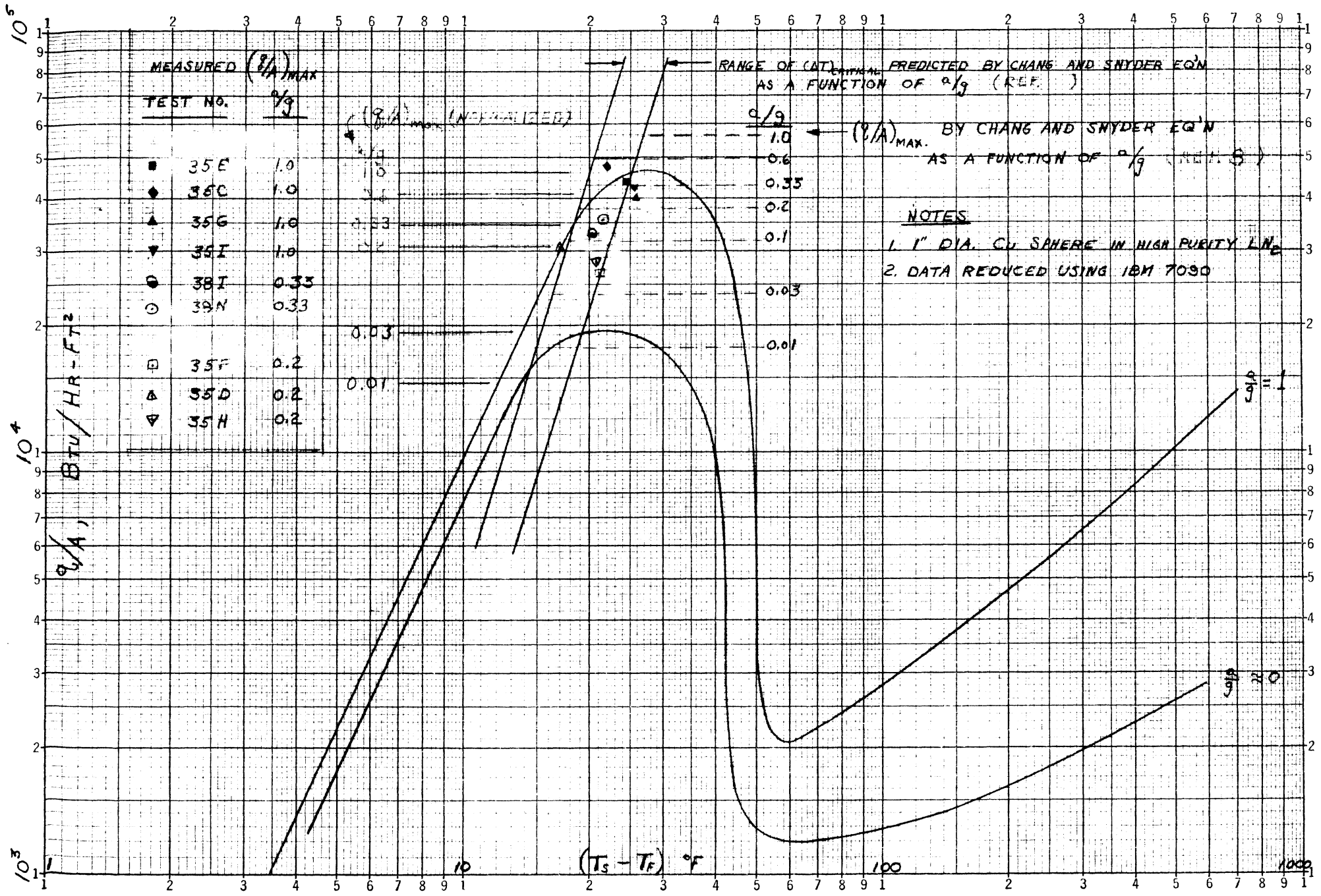

FIGURE 14. EFFECT OF a/g ON $(\Delta T)_{CRITICAL}$ AND $(q/A)_{MAX}$

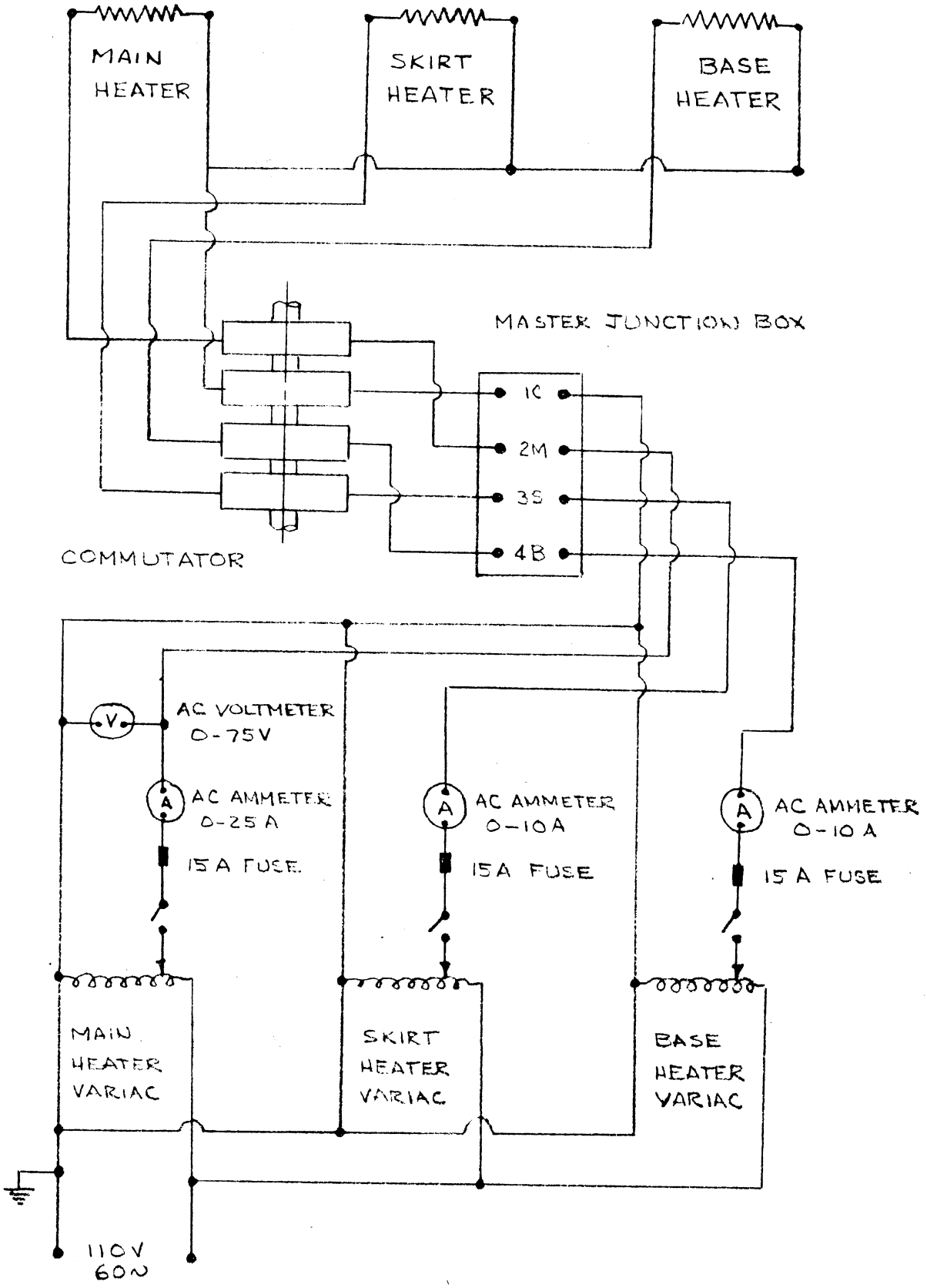

FIGURE 15. SCHEMATIC WIRING DIAGRAM FOR HEATER CIRCUIT IN LIQUID NITROGEN BOILING TEST VESSEL.

FIGURE 17 . BOILING HEAT TRANSFER DATA. RUN NO. 26
HEAT FLUX VS. HEATER SURFACE TEMPERATURE MINUS LOCAL
LIQUID NITROGEN SATURATION TEMPERATURE AT $a/g = 1.0$

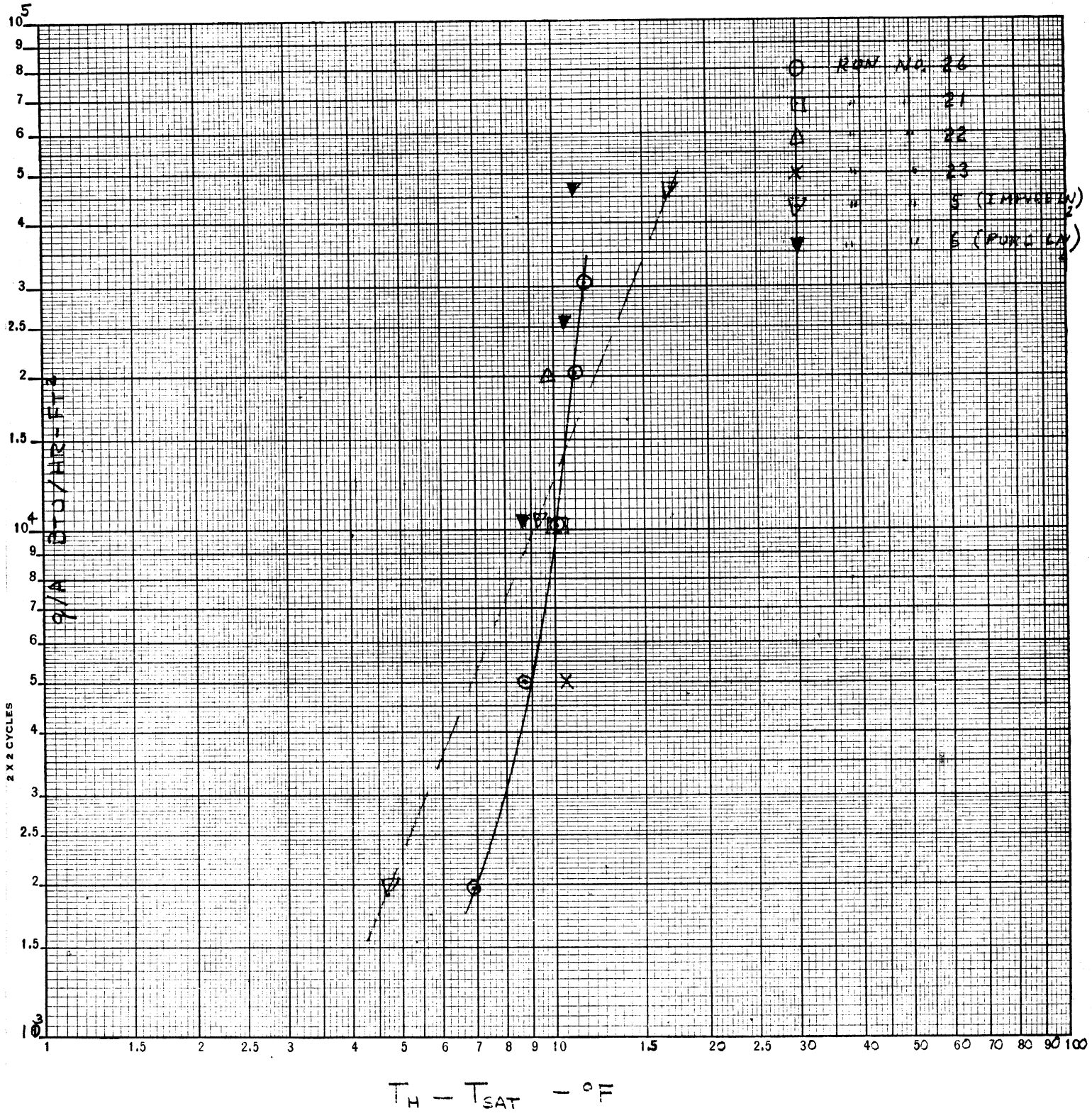

$q/A = 10,200$ BTU/HR-FT^2

RUN NO. 27

◇ $T_H - T_{SAT}$ (Heater)

⊙ $T_{W1} - T_{SAT}$ (Liquid)

⊡ $T_{W2} - T_{SAT}$ (Liquid)

NOTE: NUMBERS INDICATE SEQUENCE IN WHICH DATA WERE TAKEN.

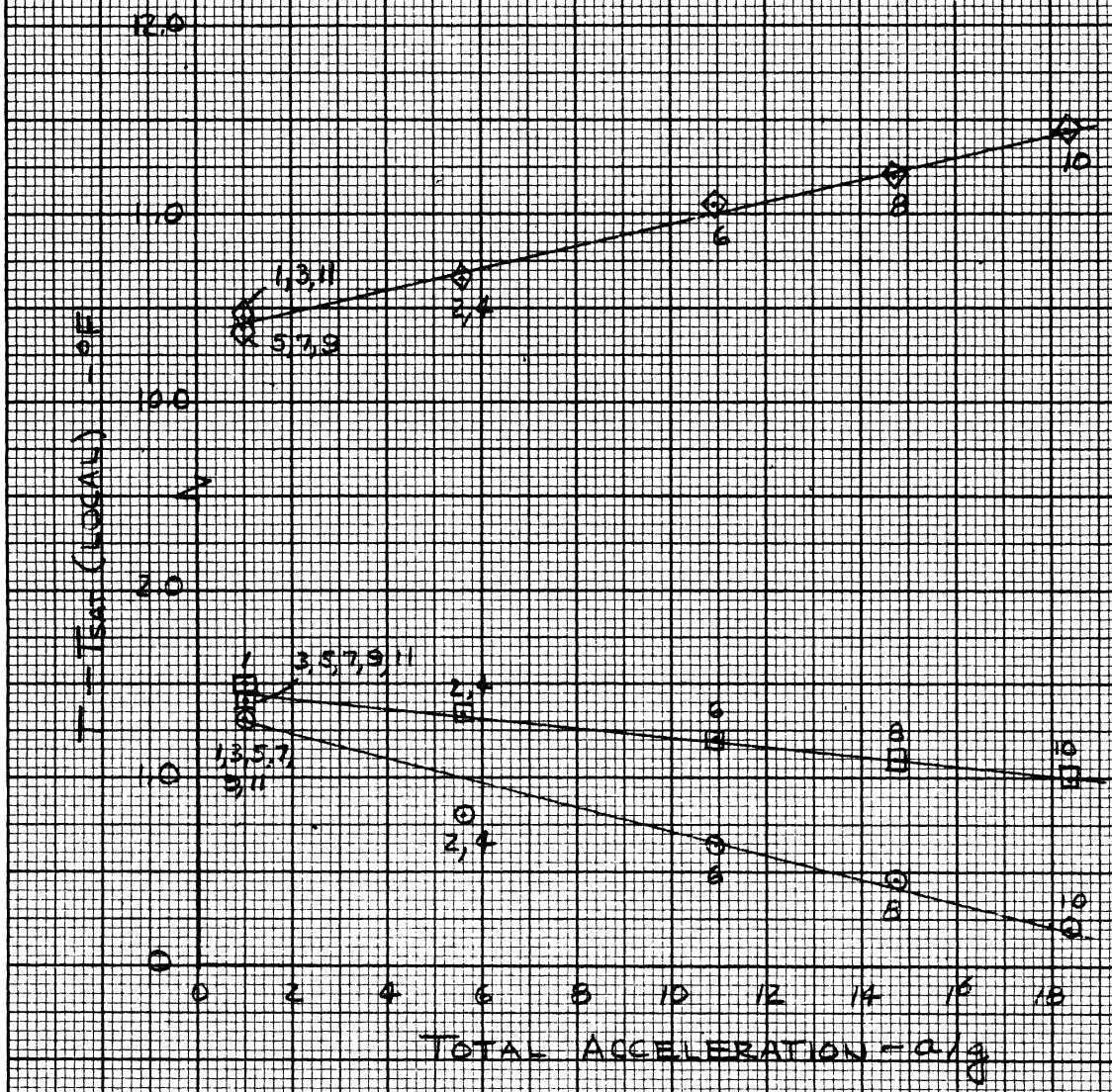

FIGURE 12. COMPOSITE PLOT FOR LIQUID ... OF 2.5 INCHES

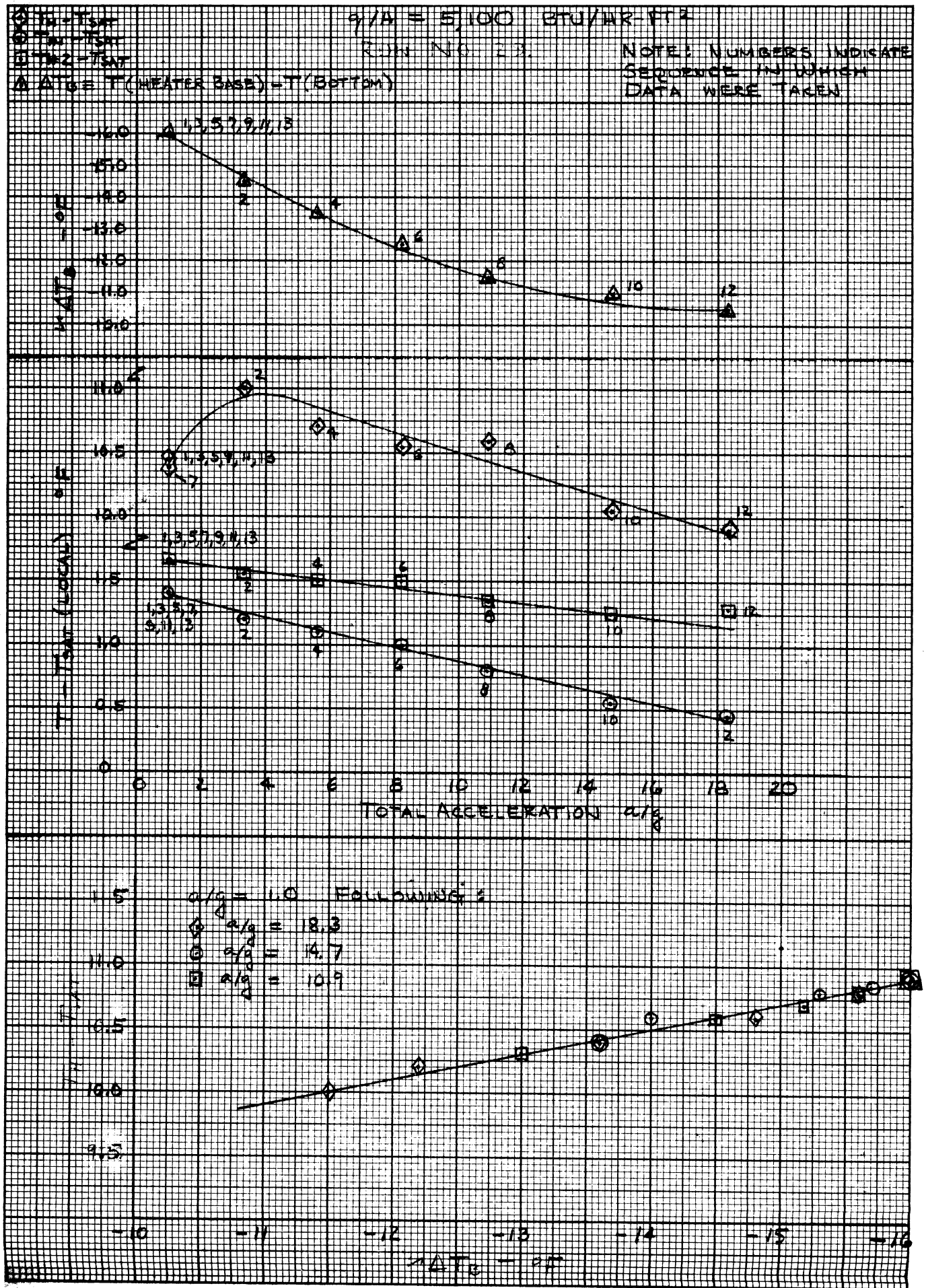

FIGURE 20. COMPOSITE PLOT FOR LIQUID DEPTH OF 2.0 INCHES

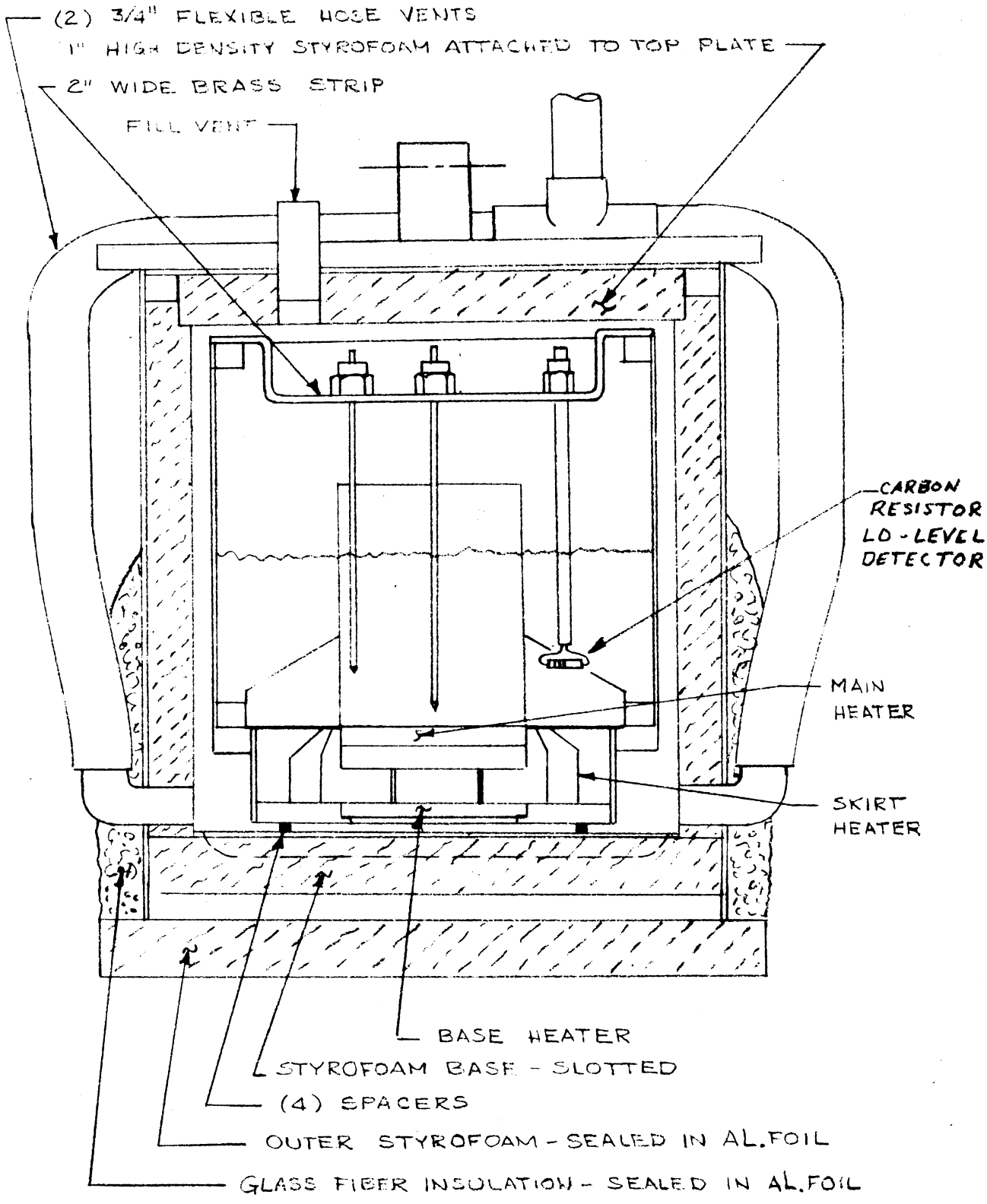

FIGURE 21. SCHEMATIC DRAWING OF LIQUID NITROGEN BOILING TEST VESSEL.

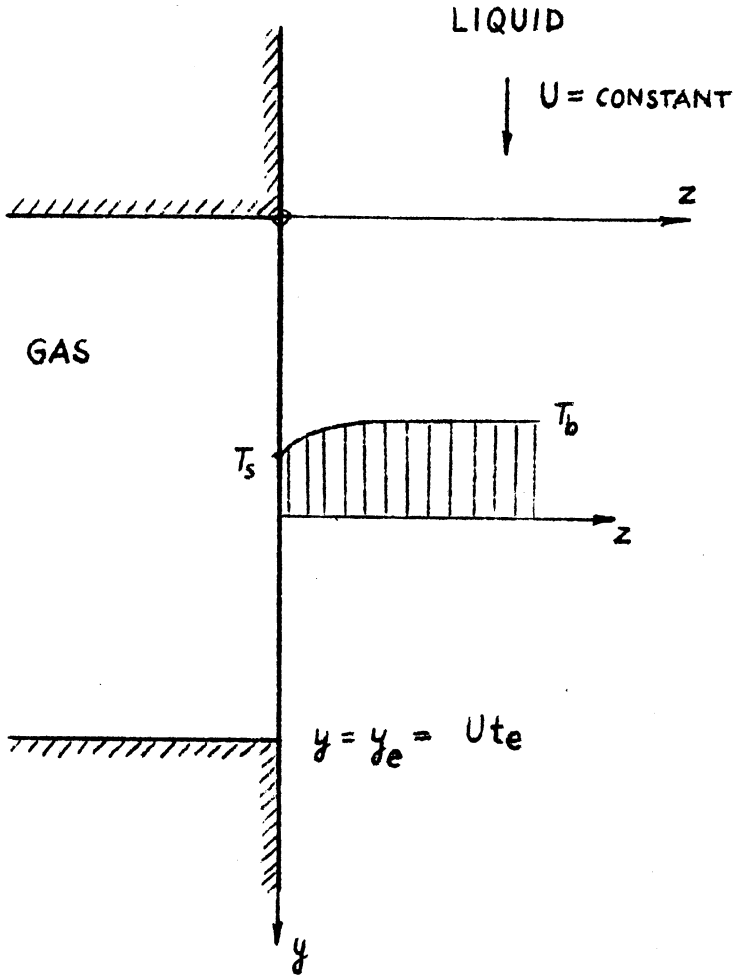

FIG. 22 ANALYTICAL MODEL FOR FALLING FILM

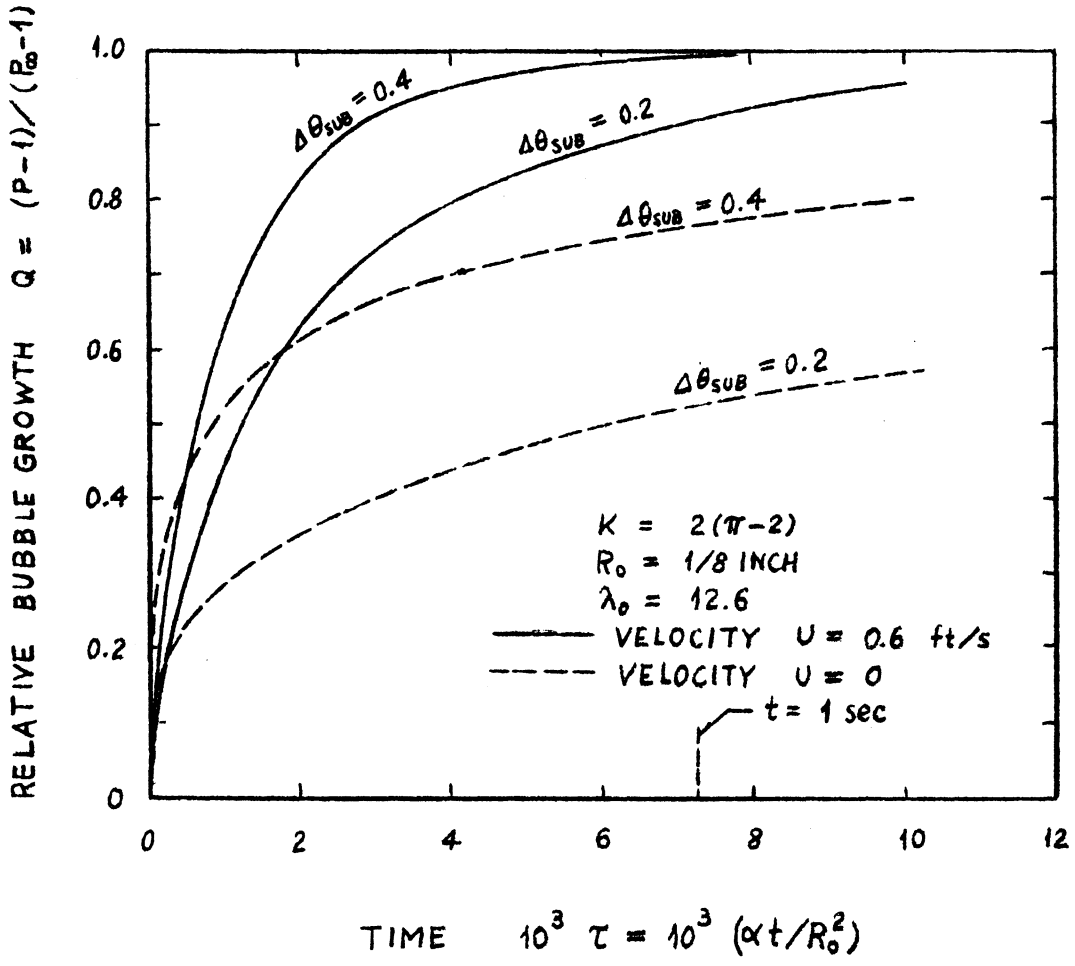

FIG. 23 RELATIVE NONDIMENSIONAL BUBBLE GROWTH LIQUID OXYGEN 3.1 atm.

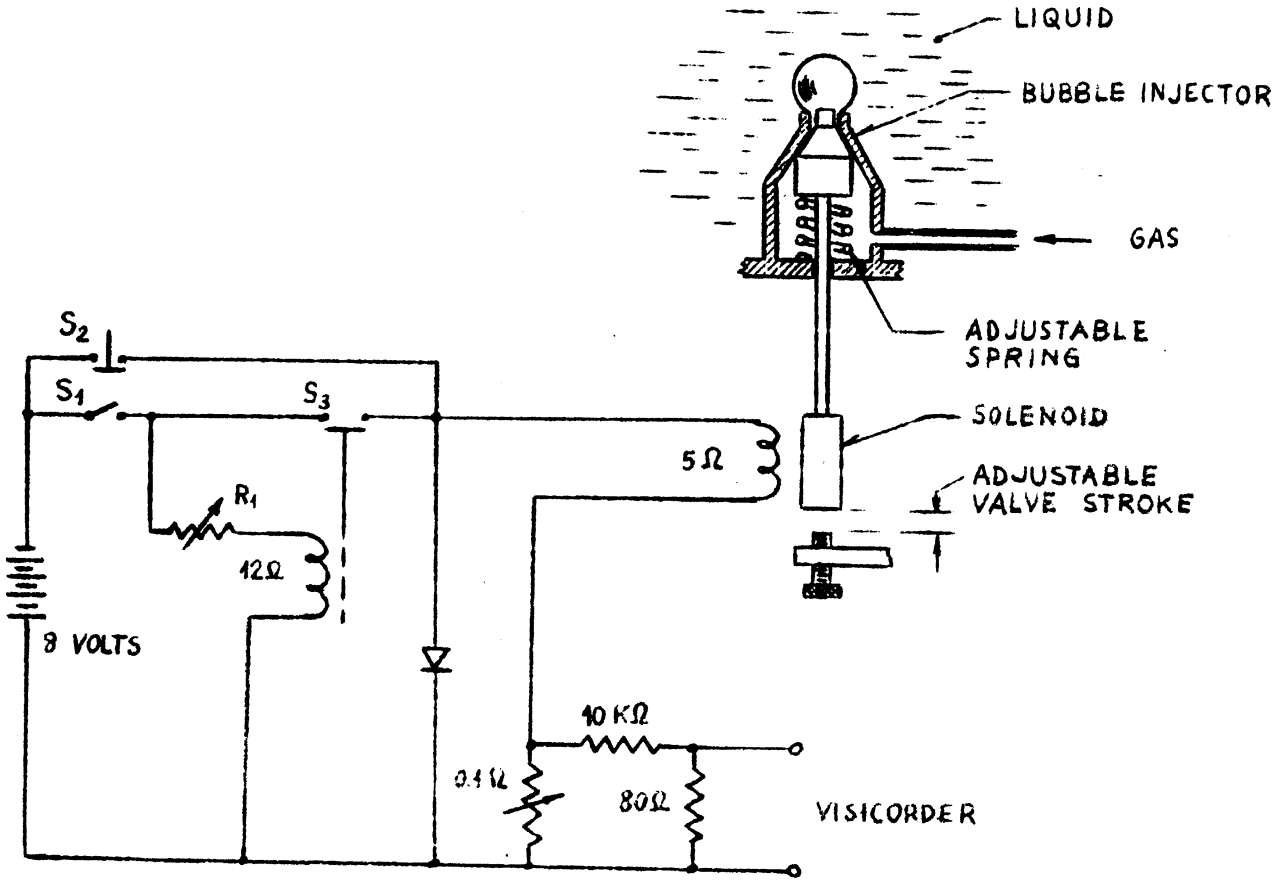

S_1 SINGLE BUBBLE FORMATION

S_2 CONTINUOUS GAS FLOW

S_3 DELAYED RELAY SWITCH, NORMAL POSITION CLOSED

FIG. 24 SWITCHING CIRCUIT ACTUATING BUBBLE INJECTOR VALVE

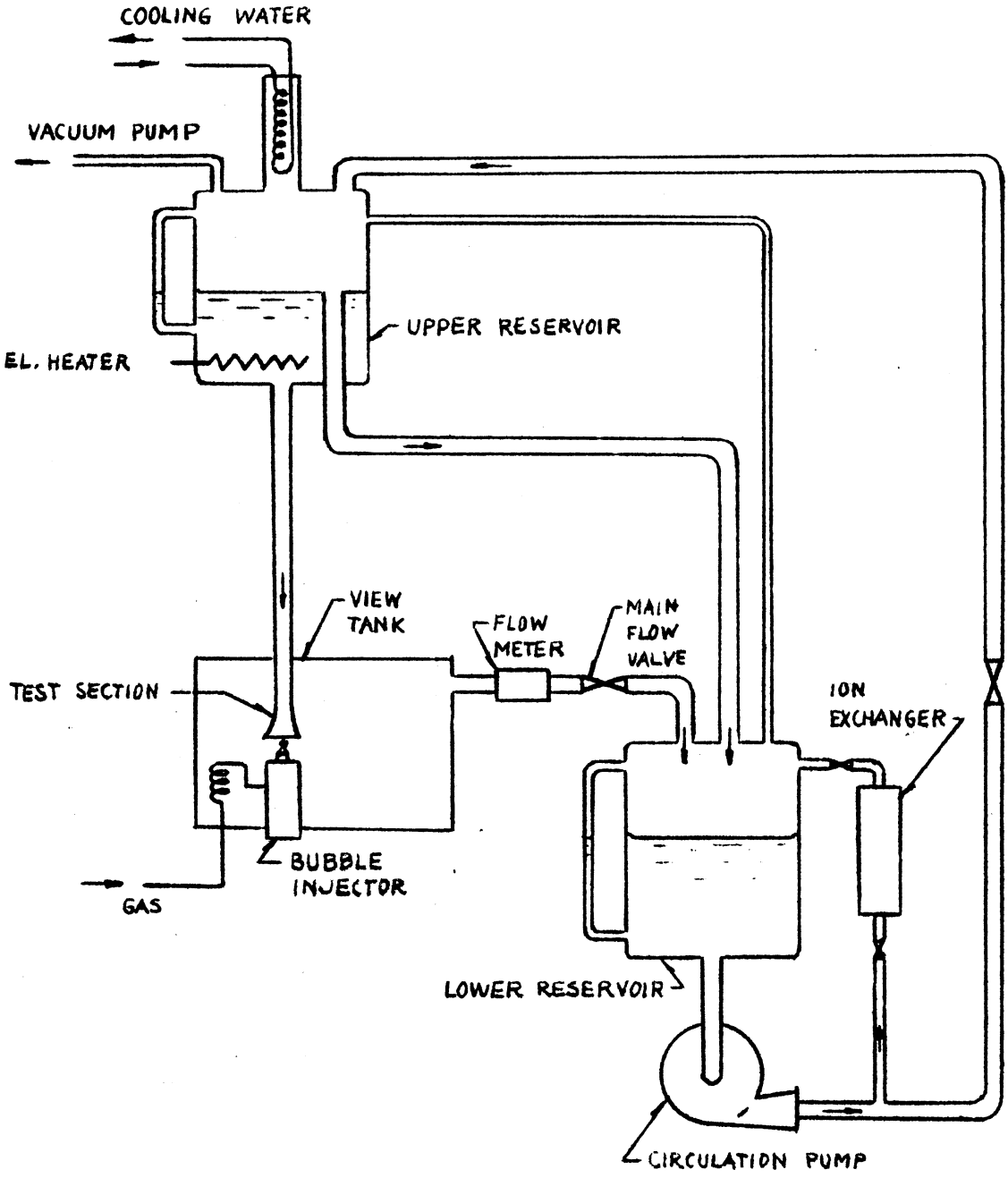

FIG. 25 FLOW DIAGRAM FOR RECIRCULATION LOOP

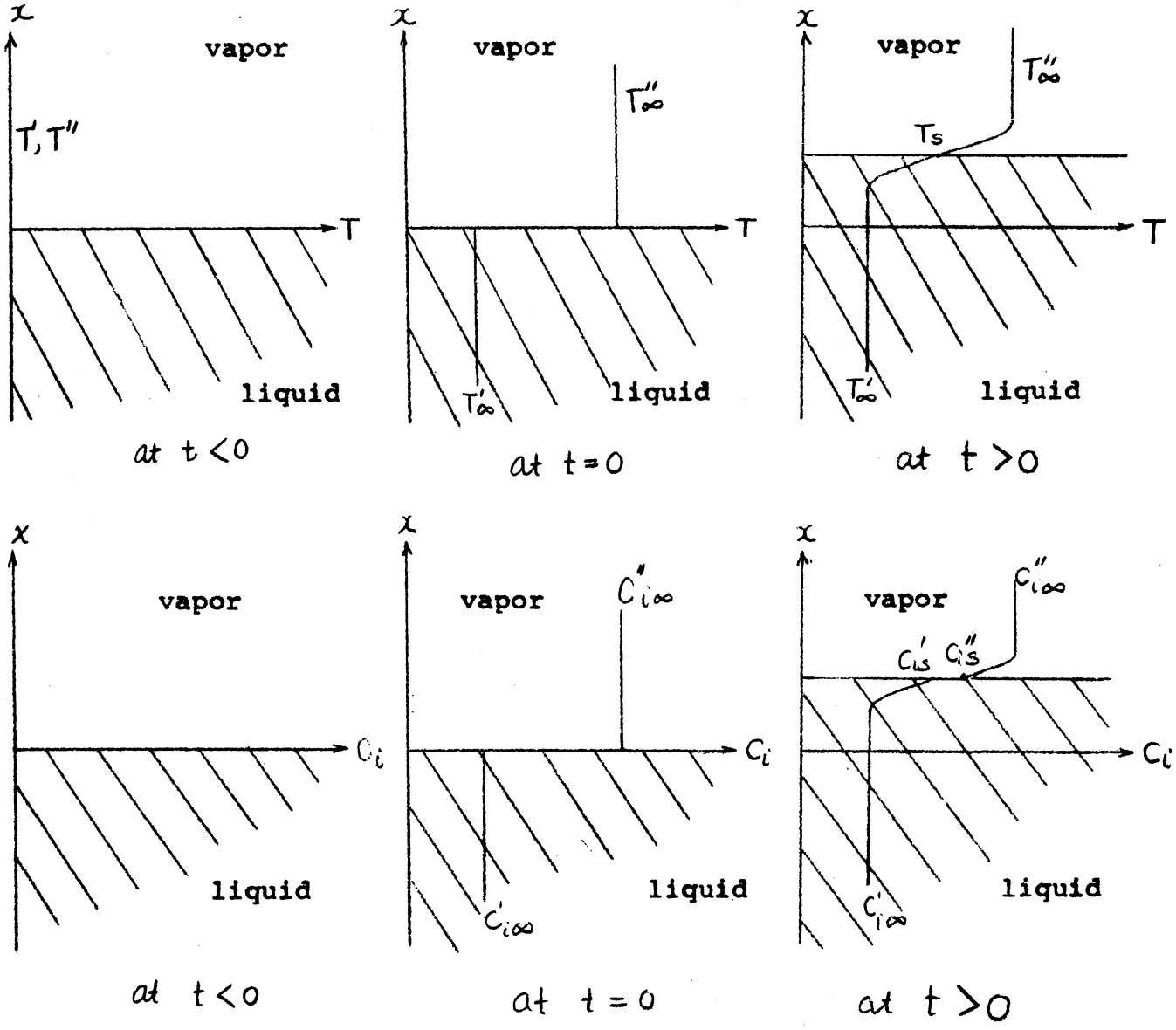

Fig. 26 Schematic Illustration of Temperature and Concentration Distributions in the Liquid and Vapor Regions at Several Different Times.

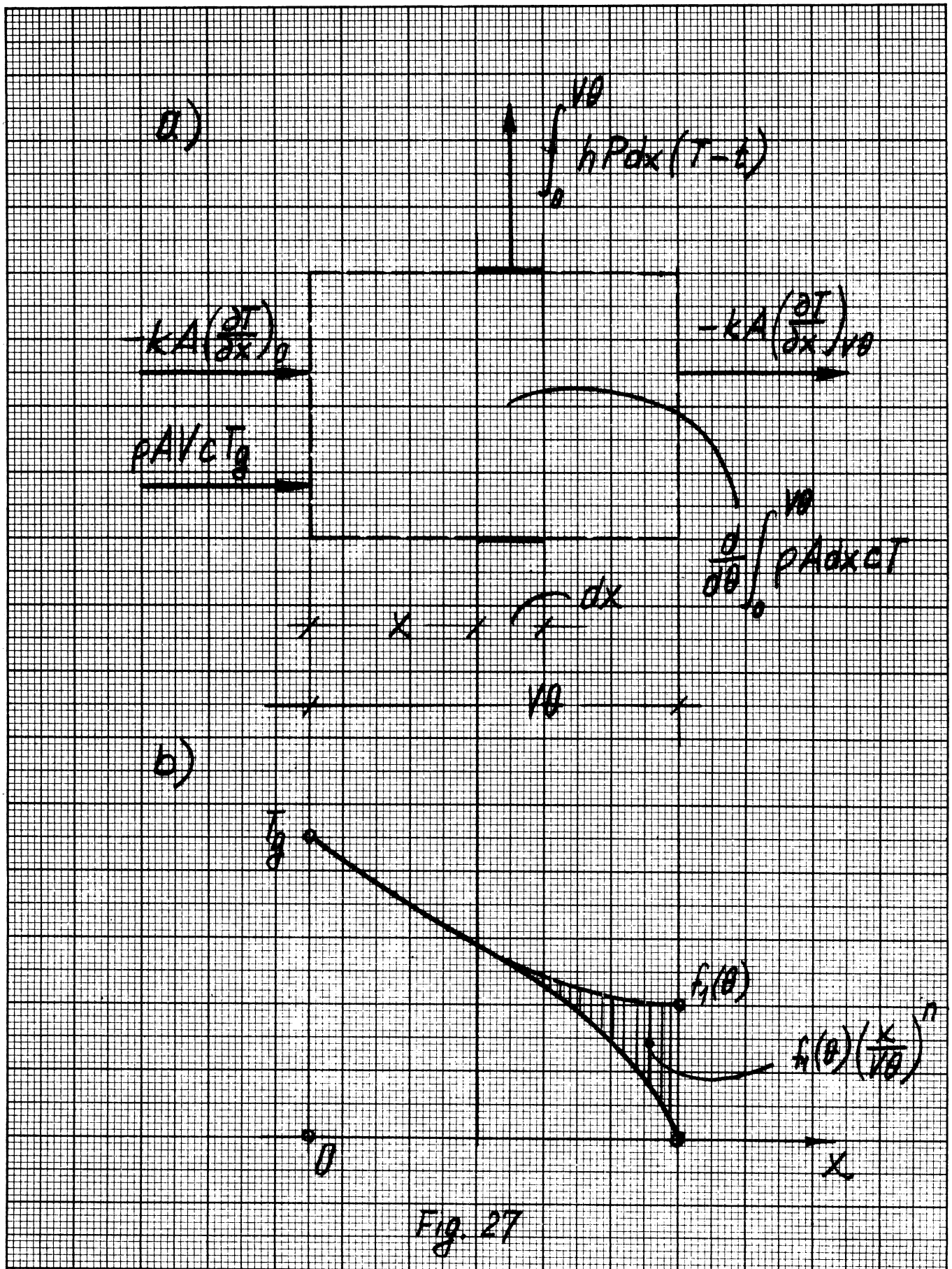

Fig. 27

The energy equation and the temperature profile for the pressurant

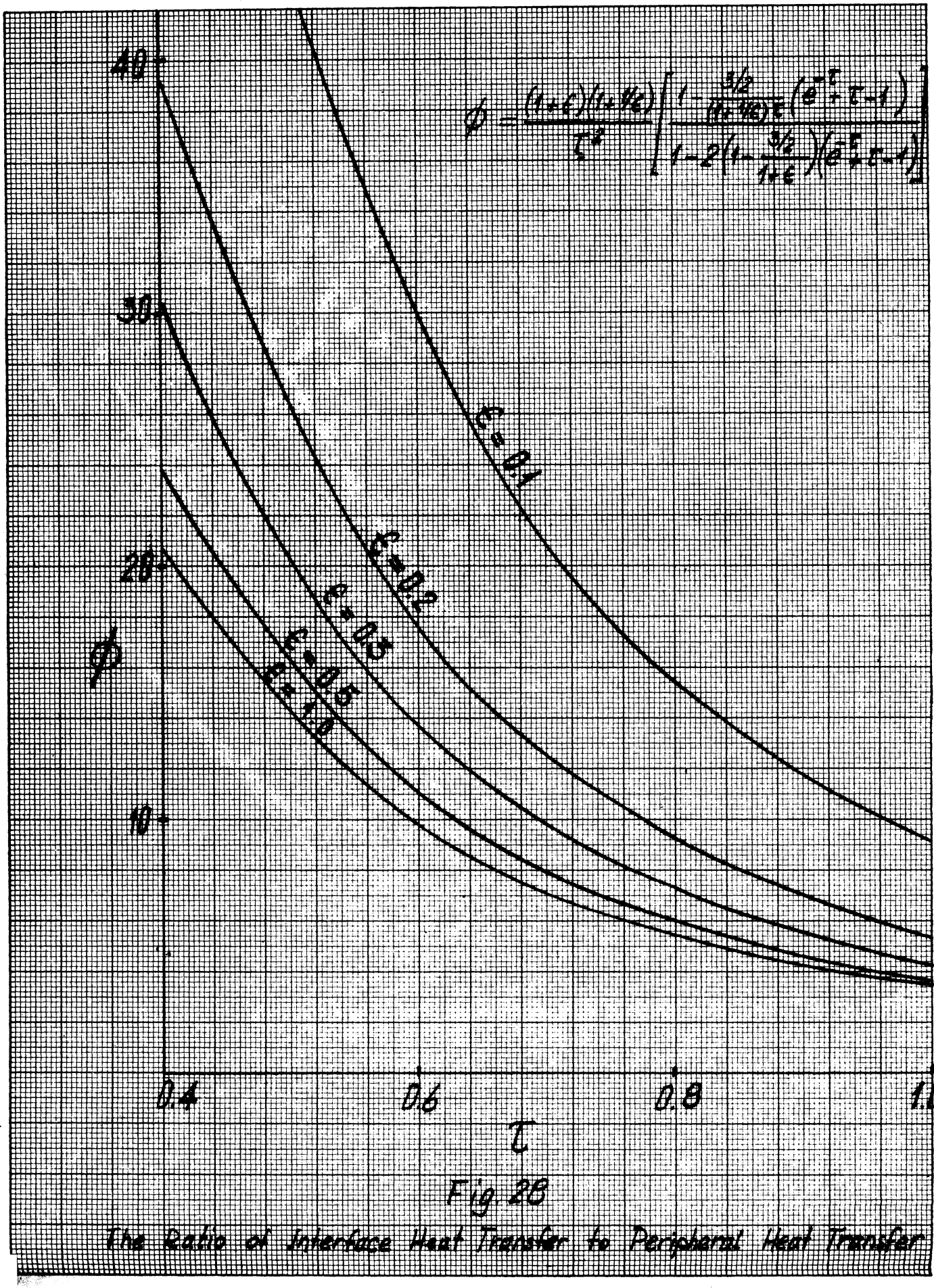

Fig. 28

The Ratio of Interface Heat Transfer to Peripheral Heat Transfer